PASSIVITY AND TIME-SCALE DECOMPOSITION TECHNIQUES FOR NONLINEAR MULTI-AGENT COORDINATION

By

Emrah Biyik

A Thesis Submitted to the Graduate

Faculty of Rensselaer Polytechnic Institute

in Partial Fulfillment of the

Requirements for the Degree of

DOCTOR OF PHILOSOPHY

Major Subject: Electrical Engineering

Approved by the
Examining Committee:

_____
Murat Arcak, Thesis Adviser

_____
John E. Mitchell, Member

_____
Arthur C. Sanderson, Member

_____
John T. Wen, Member

Rensselaer Polytechnic Institute
Troy, New York

November 2007
(For Graduation December 2007)

PASSIVITY AND TIME-SCALE DECOMPOSITION TECHNIQUES FOR NONLINEAR MULTI-AGENT COORDINATION

By

Emrah Biyik

An Abstract of a Thesis Submitted to the Graduate

Faculty of Rensselaer Polytechnic Institute

in Partial Fulfillment of the

Requirements for the Degree of

DOCTOR OF PHILOSOPHY

Major Subject: Electrical Engineering

The original of the complete thesis is on file
in the Rensselaer Polytechnic Institute Library

Examining Committee:

Murat Arcak, Thesis Adviser

John E. Mitchell, Member

Arthur C. Sanderson, Member

John T. Wen, Member

Rensselaer Polytechnic Institute
Troy, New York

November 2007
(For Graduation December 2007)

CONTENTS

LIST OF TABLES

LIST OF FIGURES

To my parents,
Nazife and Mustafa Bıyık

ACKNOWLEDGMENT

First and foremost, I'm indebted to my thesis advisor Murat Arcak for his rigorous guidance throughout my doctoral studies. He has been an excellent mentor and an inspiring example as a researcher. I also want to thank John Wen, Arthur Sanderson and John Mitchell for serving on my doctoral committee, and for their insightful comments throughout the preparation of this thesis.

My heartfelt thanks go to Kadri Özçaldıran and other faculty at Boğaziçi University in Istanbul for their encouragement to pursue graduate studies in control systems. It has been an honor to be a doctoral student at RPI. I thank all the faculty, staff and students in the ECSE Department. In addition, I appreciate the truly outstanding learning and research environment Andrzej Banaszuk, and the DyNARUM team at large, provided in United Technologies Research Center over Summer 2007.

In the last four years, I've spent countless hours in the Nonlinear and Adaptive Control Lab with Aranya Chakrabortty and Xingzhe Fan. They deserve my thanks for their friendship and for our stimulating technical discussions. Judy O'Rourke has always been cheerful and full of energy. During his visit in Fall 2005, I had fruitful discussions with Ivar-Andre Ihle, which led to some of the results in this thesis. We've followed parallel paths with Rafael Quintanilla Escalante during the doctoral process, and I've benefitted a lot from our continuous interactions.

My friends in Troy made life enjoyable. I want to thank Orhan Gürsesli for his support and friendship in my earlier years at RPI. Ali Koşar, Yusuf Artan, Murat Güven, Uma Dhanwatey, Utku Günay Acer, Çağatay Bilgin, Fikret Sivrikaya, Sertaç and Füsun Yılmaz, Ilgaz Akseli, and Ahu Aydoğan have always been there to share the joys of life.

I'm grateful to my parents Nazife and Mustafa Bıyık, and my sister Havva Esra Bıyık for their unconditional love and support throughout my life. My sister-in-law Özge Özköse brought a warm smile from Turkey and became a good friend in the last couple of months. Finally, my wife Çağrı has been the greatest inspiration to me for almost a decade, I'm privileged to have her in my life.

The research presented in this dissertation was supported in part by the National Science Foundation under grant ECS-0238268, and the Air Force Office of Scientific Research under grant FA9550-07-1-0308.

ABSTRACT

Recent years have witnessed an increasing number of feedback applications in mobile sensor networks, cooperative robotics, and vehicle formations. An essential feature of these applications is using local feedback to achieve a prescribed group behavior. Group coordination and formation control designs are utilized in a wide range of applications including autonomous sampling networks, schooling and flocking in biological organisms, optimized sensor coverage, distributed computing, drag reduction, under-way replenishment operations, safety in adversarial environments, etc.

In this thesis, we pursue nonlinear control designs that achieve group coordination. We assume a bidirectional information flow between members, and study a class of feedback laws that are implementable with local information available to each member. We first review a unifying passivity framework for the group coordination problem in continuous-time. Then, we extend it to a class of sampled-data systems by exploiting the passivity properties of the underlying continuous-time system, and prove semiglobal asymptotic stability as the sampling period and a feedback gain are reduced. We next consider a gradient climbing problem where the objective is to steer a group of vehicles to the extrema of an unknown scalar field distribution while keeping a prescribed formation. We address this task by developing a scheme in which the leader performs extremum seeking for the minima or maxima of the field, and other vehicles follow according to passivity-based coordination rules. The extremum-seeking approach generates approximate gradients of the field locally by dithering sensor positions. We show that if there is sufficient time-scale separation between the fast dither and slow gradient motions of the leader vehicle, the followers only respond to the gradient motion, and filter out the dither component, while keeping the prescribed formation.

Another major research topic in large scale systems is obtaining computationally tractable reduced order models that allow efficient simulation and analysis in the presence of varying operation conditions, parameters, etc. In this thesis, we present a time-scale separation based model reduction technique for large scale interconnected systems. We show that a two time-scale behavior can be induced by the network topology if it exhibits densely-connected clusters with sparse links across them, and prove that the dense connections cause coherent behavior to emerge within the clusters in the fast time-scale. The clusters then behave as aggregate nodes that determine the dynamic behavior of the

system in the slow time-scale. We develop a theoretical justification of the dense/sparse approach to model reduction by transforming the network model into a singularly perturbed form that makes the time-scale separation explicit. This dense/sparse approach to area aggregation complements the strong/weak approach reported in the literature, and is applicable to a number of natural and technological networks of current interest. A major advantage of this time-scale approach to aggregation is its appeal to physical intuition, which can be lost in reduced models constructed merely for algebraic or numerical efficiency.

CHAPTER 1
INTRODUCTION

The main challenge in cooperative control applications for multi-agent systems is to achieve a prescribed group behavior with local feedback rules, rather than with centralized controllers. For formation stability such local feedback rules have been derived from artificial attraction and repulsion forces with neighboring vehicles [1, 2, 3]. Formation designs are utilized in a variety of applications including autonomous sampling networks, optimized sensor coverage, under-way replenishment operations, drag reduction, and safety in adversarial environments. Agreement problem, where the objective is to steer variables of interest (position, heading angle, phase of oscillations, etc.) to a common value across the network has also attracted a wide interest in the literature [4, 5, 6, 7, 8]. The agreement problem finds applications in distributed computing [9], schooling and flocking in biological organisms [10, 11], and forest fire surveillance [12], among others. For unidirectional communication topologies numerous results have been obtained for certain classes of feedback laws using a number of different approaches, such as the use of Laplacian properties for directed graphs in [6, 13], input-to-state stability in [14], eigenvalue structure of circulant matrices in [15], and set-valued Lyapunov theory in [7]. Decentralized protocols achieving consensus under switching (time-varying) network topologies are also studied in several research papers, *e.g.* [6, 7, 16, 17, 18]. Some preliminary results for coordination problems in the presence of time-delays, which are inevitable in most networked systems, are obtained using tools from robust linear control [6], and convex analysis [19].

Another topic of interest in large scale systems research is obtaining reduced order models for large scale systems is because, as the number of nodes in a network of sensors, vehicles, power generators, etc. grows, analysis, control design, and simulation for the dynamic model become computationally prohibitive. A time- scale separation approach, developed in the 70's for large-scale power networks, took advantage of the differing strength of interactions between the generators to decompose the network into slow and fast reduced-order models [20, 21, 22]. As revealed by a singular perturbation analysis in [20], groups of strongly interacting generators synchronize in the fast time-scale according to a model that treats the weak connections as perturbations. Over a longer period, however, the weak interactions become significant and govern the slow time-scale behavior of the groups, which are now treated as aggregate nodes. This time-scale sepa-

ration approach found use in numerous applications, and was further extended to reduce the order of finite state Markov chains that exhibit weak transition probabilities between groups of strongly interacting states [23, 24, 25]. A major advantage of this time-scale approach to aggregation is its appeal to physical intuition, which can be lost in reduced models constructed merely for algebraic or numerical efficiency.

A time-scale separation can be induced by the network topology even when the strength of the interactions between the nodes are uniform. We show in Chapter 5 that if the network exhibits a clustered interconnection structure as in Figure 5.1, then a coherent behavior emerges within the clusters in the fast time-scale. The clusters then behave as aggregate nodes that model the slow dynamics of the system. Clustered networks are common in biology as discussed in [26], and have been reported in cellular signalling networks [27], cell-cycle regulatory networks [28, 29], metabolic networks in E. coli [30], and in foraging insects [31, 32]. Among other engineering systems, a clustered structure is favorable in sensor network design because it is suitable for efficient routing and broadcasting protocols, and because it affords significant savings in bandwidth and power [33].

1.1 Preview of the Dissertation

We build on a passivity framework for group coordination and agreement, developed in [17], which provides ample design flexibility, and encompasses many of the results in the literature, *e.g* [1, 6], as special cases. Below we summarize the main contributions of this thesis:

1.1.1 Passivity Based Group Coordination: Overview

In Chapter 2 we review the recent passivity framework for group coordination presented in [17]. We first formulate a coordination problem that is applicable to formation stabilization and group agreement as special cases, and present a class of feedback laws that solve this problem with local information. These feedback laws assume that, if a communication link exists between two members of the group, then both members gain access to each others information. A key observation in [17] is that such bidirectional communication gives rise to a special interconnection structure which guarantees that the resulting feedback loop will inherit the passivity properties of its components. By exploiting this structure, [17] develops a design method which results in a broad class of feedback laws that achieve passivity and, thus, stability of the interconnected system. The passivity approach also leads to a systematic construction of a Lyapunov function in the form of a

sum of storage functions for the subsystems. As detailed in [17], several existing feedback rules for formation stability and group agreement become special cases in the passivity framework.

1.1.2 Synchronized Path Following: A Sampled Data Design

Sampled-data implementation in cooperative control is of practical importance, because data exchange between members is carried out over a communication channel. Although data is transmitted in discrete-time, controllers and internal dynamics of the agents may be continuous-time, which means that a sampled-data analysis of the feedback system is necessary. In Chapter 3, we exploit the passivity property of the underlying continuous-time plant and make use of results from [34] on the preservation of dissipativity properties under sampling. Our main result establishes semiglobal asymptotic stability as the sampling period and a feedback gain are reduced. One of the motivations for this study is a path-following problem studied in [35] where the path parameters are to be synchronized for vehicles in a formation. In this application the path parameters may be updated in discrete-time, while the path-following controllers may be implemented locally in continuous-time, thus resulting in a sampled-data feedback system that fits our framework.

1.1.3 Gradient Climbing in Formation

A central problem in cooperative control is "gradient climbing" [2, 3, 36, 37] in which robotic vehicles search for minima or maxima of a field distribution (*e.g.* to locate and repair an oil leak). We address this task by combining potential function methods for maintaining a relative configuration between vehicles, and *extremum seeking* methods for steering them to the extrema of the unknown field. Earlier applications of extremum seeking to formation flight in [38, 39] aim to maximize the induced lift for the wingman, and do not address the search of a field distribution. Classical extremum seeking tools, modernized and refined in [40, 41, 42], locate the extrema of an output function by systematically perturbing the input parameters, and by making an on-line estimation of the gradient of the output relative to these inputs.

Unlike the sensor coverage problem in [37] and the least-squares gradient estimation proposed in [2, 36], which rely on multiple sensor information, the extremum-seeking approach presented in Chapter 4 generates approximate gradients locally, by *dithering* sensor positions. The advantage of this local approximation is that only designated leaders

need sensing capabilities, and communication of sensed variables and geographic proximity of sensors are not necessary for generating approximate gradients. Indeed, it is noted in [43] that E. coli bacteria perform a similar dynamic sampling process to individually estimate gradients for foraging. Our leader-only sensing scheme is advantageous in applications where the sampling process is expensive, *e.g.* in monitoring contamination of sediments [44].

One of the mainstream approaches in extremum-seeking design is to probe the system with sinusoidal inputs, and to make an on-line estimation of the gradient of the output relative to these inputs [40]. An alternative approach relies on nonlinear optimization techniques to estimate the gradient information in discrete-time [41]. Earlier applications of extremum seeking to formation flight in [38, 39] aim to maximize the induced lift for the wingman, and do not address the search of a field distribution. Recent papers [45, 46] address source seeking of a single vehicle by employing continuous-time extremum seeking methods. The vehicle uses a sinusoidal perturbation to compute the gradient of the field and updates its velocity accordingly in continuous-time.

In Chapter 4, the leader performs extremum seeking for the field minima or maxima, and other vehicles follow according to potential-based coordination rules. Keeping a group formation during the transients may be desirable for reliable inter-vehicle communication/sensing or drag reduction. Another example of a leader-following based formation design is presented in [47] where the followers carry a load cooperatively in a planetary terrain exploration mission.

For stability of our extremum-seeking scheme a judicious tuning of the design parameters is critical: There must be sufficient time scale separation between the gradient update and the frequency of dither. The dither frequency must also be large enough that the followers only respond to the slow gradient motion of the leader, and filter out the dither component. To systematically tune the gains, step size, dither size and frequency parameters, we employ the *two-time-scale averaging* tools in [48] and their applications to extremum seeking in [42]. Although our formulation differs from the studies [40, 41, 42] where the function to be optimized is the steady-state map of a dynamic system, the two-time-scale averaging framework is still suitable because the formation dynamics relative to the leader play the role of the boundary-layer system in a singularly perturbed model.

1.1.4 Area Aggregation and Time-Scales in Sparse Nonlinear Networks

One of the most significant problems in large-scale systems research is the prediction of the dynamic behavior for the full network from a computationally tractable reduced-order model. A powerful approach for the development of such reduced models is to exploit the separation of time scales that arise due to differing strengths in the connections between the components. A time-scale decomposition methodology was developed in the 70's for large power systems, and reduced network models for long term behavior were obtained by representing each coherent area with a single "equivalent machine" [20, 21, 22]. Analogous results exist in large economic models where, in the long run, each sub-economy is represented by a single aggregate price, which is then used to study the interaction between these sub-economies [49].

In Chapter 5 we show that a time-scale separation also results from a sparse interconnection structure where coherent areas are now characterized by internally dense and externally sparse interconnections. Indeed, extending an original idea in [50] for power networks, we show that if the network exhibits densely-connected clusters with sparse links across them as in Figure 5.1, then the dense connections cause coherent behavior to emerge within the clusters in the fast time scale. The clusters then behave as aggregate nodes that determine the dynamic behavior of the system in the slow time scale. We first derive a singular perturbation model which makes this time-scale separation explicit and, next, prove the validity of the reduced-model approximation on the infinite time interval. Our result in Chapter 5 is applicable to nonlinear networks and encompasses as a special case the linear study of [50]. It further employs modern tools from algebraic graph theory and provides new insights on the structure of the singular perturbation decomposition, even for the linear case. The nonlinear result is made possible by a new set of slow and fast variables motivated by the graph Laplacian, and by a recent singular perturbation approximation result in the infinite time interval due to Khalil [51].

1.2 Methodology

In this thesis we use a broad range of technical tools from nonlinear control theory (such as sampled-data analysis, singular perturbations, dissipativity) and unconstrained optimization. We either use standard results to prove the validity of our designs, or extend them to obtain new tools that are applicable to our problems. In the remainder of this section, we overview the main technical tools.

1.2.1 Dissipativity

In the early 60's, the notion of positive realness from circuit theory [52] gained a major role in systems and control theory through the celebrated positive real (or KYP) lemma [53, 54, 55]. In [56] Willems conceptualized dissipativity by introducing *storage functions* and *supply rates*.

Consider the dynamic system

$$\begin{aligned} \dot{x} &= f(x,u) \\ y &= h(x,u), \quad x \in R^n,\ u,y \in R^p \end{aligned} \tag{1.1}$$

endowed with a function $w : R^m \times R^p \to R$ called the *supply rate*. Then the system (1.1) is said to be *dissipative* with respect to the supply rate w if there exists a positive definite function $S : R^n \to R^+$, such that for all $x(t_0) \in R^n$, all $T > t_0$, and all input functions u

$$S(x(T)) \leq S(x(t_0)) + \int_{t_0}^{T} w(u(t), y(t))dt \tag{1.2}$$

where $x(T)$ is the state of (1.1) at time $t = T$ resulting from initial condition $x(t_0)$ and $u(\cdot)$

The inequality (1.2) is called the dissipativity inequality. It implies that the stored energy $S(x(T))$ of (1.1) at any future time T is at most equal to the sum of the stored energy $S(x(t_0))$ at present time and the total externally supplied energy $\int_{t_0}^{T} w(u(t), y(t))dt$ during the interval $[t_0, T]$. Hence, there can be no internal creation of energy; only internal *dissipation* of energy is possible.

A special class of dissipative systems is *passive* systems, where the supply rate is $w = u^T y$. In this case, there exists a positive semidefinite storage function $S(x) \geq 0$ such that

$$\dot{S} = \nabla S(x)^T f(x,u) \leq -Q(x) + u^T y \tag{1.3}$$

for some positive semidefinite function $Q(x)$. We say that (1.1) is strictly passive if $Q(x)$ is positive definite. A static nonlinearity $y = h(u)$ is passive if, for all $u \in R^p$,

$$u^T y = u^T h(u) \geq 0; \tag{1.4}$$

and strictly passive if (1.4) holds with strict inequality $\forall u \neq 0$. Likewise, storage functions of the forms $w(u,y) = u^T y - \alpha u^T u$ and $w(u,y) = u^T y - \beta y^T y$, $\alpha, \beta > 0$ lead to *input*

strictly passive, and *output strictly* passive systems, respectively.

The notion of passivity has been instrumental in the development of absolute stability criteria in the 60's, in adaptive control and large-scale system studies in the 70's and 80's, as well as in the nonlinear control design procedures developed in the 90's [57]. The use of passivity as a nonlinear stabilization tool was made possible by the Passivity Theorem of Popov [55] and Zames [58], which states that the feedback interconnection of two nonlinear passive blocks F1 and F2 as in Figure 1.1 is stable.

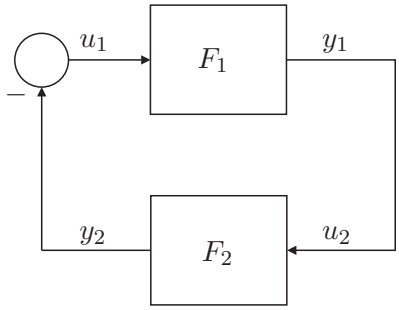

Figure 1.1: Feedback interconnection of two passive blocks is stable

A useful property is that pre-multiplication by an arbitrary matrix D and post-multiplication by its transpose D^T as in Figure 1.2 does not change the passivity properties of the passive block F. This property is essential in proving stability of large-scale decentralized systems with symmetric interconnections.

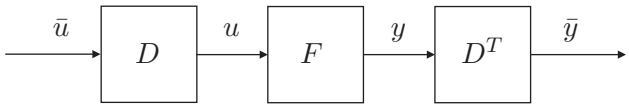

Figure 1.2: Pre-multiplication by D and post-multiplication by D^T does not change the passivity properties of F

1.2.2 Sampled-Data Analysis

While nonlinear control theory is developed mainly for continuous-time systems, the wide use of digital controllers calls for the study of sampled-data systems. Sampled-data control studies can be classified into two main approaches. In the first approach, a continuous-time controller is designed using the continuous-time model, and then discretized and implemented using sample/hold devices [59, 60, 61, 34]. The second approach is to approximate the nonlinear plant by a discrete-time model, and then design a discrete-

time controller [62, 63, 64, 65]. Because the exact discrete-time model of the underlying continuous-time plant is seldom available in nonlinear systems, the sampled data studies in [59]-[66] determine stability from properties of the continuous-time model. This approach typically yields "semiglobal" asymptotic stability results, which show that the region of attraction enlarges as the sampling period and possibly other design parameters are reduced.

In [59], for sufficiently small sampling period T, it is shown that a sampled-data controller achieves semiglobal practical stabilization; that is, for every compact set of initial conditions and every tolerance $\epsilon > 0$, there exists a T^* such that for all $T < T^*$, the closed-loop trajectory $||x(t)||$ is ultimately bounded by ϵ. It is shown in [67] and [68] that discrete-time implementation of an exponentially stabilizing continuous-time state feedback controller yields $\lim_{t\to\infty} x(t) = 0$. The presence of bounded disturbances are studied in [66], and, under an exponential stability assumption, it is shown that sampled-data controller achieves practical stabilization. Moreover, the ultimate bound approaches the one under continuous-time control as $T \to 0$, which means that we recover $\lim_{t\to\infty} x(t) = 0$ in the absence of disturbance. Reference [34] studies a class of continuous-time controllers that render a certain dissipation inequality satisfied globally in the presence of disturbance inputs. The controller is then discretized and implemented using zero-order hold. It is shown that, for sufficiently small T, the sampled-data controller recovers the disssipation inequality in a semiglobal practical sense. When specialized to the stabilization problem, the results of [34] show semiglobal practical stabilization of the exact discrete-time model, and the conclusion extends to inter-sampling behavior by employing results from [69].

1.2.3 Two-Time Scale and Averaging Methods

Suppose we are given the state equation $\dot{x} = f(t, x, \epsilon)$ where ϵ is a small positive parameter, and suppose the equation has the solution $x(t, \epsilon)$. The goal of an asymptotic method is to obtain an approximate solution $\tilde{x}(t, \epsilon)$ such that the approximation error $x(t, \epsilon) - \tilde{x}(t, \epsilon)$ is small, in some norm, for small ϵ and the approximate solution $\tilde{x}(t, \epsilon)$ is expressed in terms of equations simpler than the original equation. The practical significance of asymptotic methods is in revealing underlying multiple-time-scale structures inherent in many applications. Quite often the solution of the state equation exhibits the property that some variables move in time faster than other variables, leading to the classification of variables as *slow* and *fast*. Both the averaging method and the singular

perturbation method deal with the interaction of slow and fast variables.

Averaging method was initially proposed by Bogoliuboff and Mitropolsky in [70]. It was further developed in [71] and [72], and extended to geometric form in [73] and [74]. The averaging method is widely used in extremum seeking problems [40, 75], where the periodic sinusoidal perturbation is averaged out by the plant dynamics.

Singular perturbation theory was originally developed as an analysis tool for fluid dynamics and nonlinear mechanics. It was recognized in 60's that singular perturbations are present in most control schemes based on reduced models which disregard the high gain/high frequency *parasitics*. This recognition led to the development of time-scale methods for a variety of applications including trajectory optimization [76, 77], stochastic modeling, estimation and control [78, 79], high gain feedback systems [61, 80, 81], power networks [22, 20], aggregation of Markov chains [82], and modeling and stability of large scale systems [21].

1.2.3.1 Averaging

The averaging method is applicable to a system of the form

$$\dot{x} = \epsilon f(t, x, \epsilon) \tag{1.5}$$

where ϵ is a small positive parameter and $f(t, x, \epsilon)$ is periodic in t with period T; that is,

$$f(t, x, \epsilon) = f(t + T, x, \epsilon)$$

for all x and ϵ. We assume that f is sufficiently smooth in its arguments over the domain of interest. The method approximates the solution of (1.5) by the solution of the autonomous *averaged* system

$$\dot{x} = \epsilon f_{av}(x), \tag{1.6}$$

where

$$f_{av}(x) = \frac{1}{T} \int_0^T f(\tau, x, 0) d\tau. \tag{1.7}$$

The solution of the averaged system (1.6) provides an $\mathcal{O}(\epsilon)$ approximation for the solution of (1.5) over some finite time interval $[0, a]$. If the averaged system in (1.6) has an exponentially stable equilibrium point $x^* = p$, then there is a domain $\mathcal{D} := \{x : ||x - p^*|| < \rho\}$, for some $\rho > 0$, such that for all $x(0) \in \mathcal{D}$, the $\mathcal{O}(\epsilon)$ approximation is valid for all

$t \geq 0$.

The averaging method can be extended to systems where the right-hand side of (1.5) is not periodic in t, if an average of $f(t, x, 0)$ can be defined by the limit

$$f_{av}(x) = \lim_{T \to \infty} \frac{1}{T} \int_t^{t+T} f(\tau, x, 0) d\tau.$$

A simple example is in the case when $f(t, x, \epsilon) = f_1(t, x, \epsilon) + f_2(t, x, \epsilon)$, where f_1 is periodic in t while f_2 decays to zero as t tends to infinity, uniformly in (x, ϵ).

1.2.3.2 Singular Perturbation

We consider the singularly perturbed system

$$\dot{x} = f(t, x, z, \epsilon), \tag{1.8}$$

$$\epsilon \dot{z} = g(t, x, z, \epsilon), \tag{1.9}$$

where setting $\epsilon = 0$ degenerates the differential equation $\epsilon \dot{z} = g(t, x, z, \epsilon)$ into the algebraic or transcendental equation $0 = g(t, x, z, 0)$. The essence of the singular perturbation theory is that the discontinuity of solutions caused by singular perturbations can be avoided if analyzed in separate time-scales. This multi-time-scale approach is a fundamental characteristic of the singular perturbation method.

We assume the functions f and g are sufficiently smooth in the domain of interest, and let $z := h(t, x)$ denote the isolated solution of the quasi-steady-state equation

$$0 = g(t, x, z, 0), \tag{1.10}$$

obtained by letting $\epsilon = 0$ in (1.9). Then the *reduced model* is given as

$$\dot{x} = f(t, x, h(t, x), 0). \tag{1.11}$$

Singular perturbations cause a two-time-scale behavior characterized by the presence of slow and fast transients in the system's response. The slow response is approximated by the reduced model (1.11), while the discrepancy between the response of the reduced model (1.11) and that of the full model in (1.8)-(1.9) is the fast transient.

To analyze the behavior of z during the fast transient, we let $y := z - h(t, x)$ and

$\tau := \frac{t}{\epsilon}$, then in the τ time scale y satisfies the equation

$$\frac{dy}{d\tau} = g(t, x, y + h(t, x), \epsilon) - \epsilon \frac{\partial h}{\partial \tau} - \epsilon \frac{\partial h}{\partial \tau} f(t, x, y + h(t, x), \epsilon), \tag{1.12}$$

The variables t and x are now slowly varying in the τ time-scale. Setting $\epsilon = 0$ reduces equation (1.12) to the *boundary-layer model*

$$\frac{dy}{d\tau} = g(t_0, x, y + h(t, x), 0), \tag{1.13}$$

where (t, x) are now fixed parameters, and which has an equilibrium at $y = 0$.

When the origin of the boundary layer system in (1.13) is exponentially stable, uniformly in the frozen parameters (t, x) the fundamental result of singular perturbation theory, known as *Tikhonov's Theorem* states that if the reduced problem in (1.11) has a unique solution $\bar{x}(t)$, defined on $[t_0, t_1]$, then for sufficiently small ϵ, the full problem (1.8)-(1.9) has a unique solution $(x(t, \epsilon), z(t, \epsilon))$ defined on $[t_0, t_1]$ and

$$x(t, \epsilon) - \bar{x}(t) = \mathcal{O}(\epsilon), \tag{1.14}$$

$$z(t, \epsilon) - h(t, \bar{x}(t)) - \hat{y}(t/\epsilon) = \mathcal{O}(\epsilon), \tag{1.15}$$

hold uniformly for $t \in [t_0, t_1]$, where $\hat{y}(\tau)$ is the solution of the boundary layer model in (1.13). Moreover, if the reduced model has an exponentially stable origin, then the approximation results in (1.14)-(1.15) hold in the infinite-interval, i.e. with $t_1 = \infty$.

CHAPTER 2
PASSIVITY-BASED GROUP COORDINATION: OVERVIEW

2.1 Problem Statement

Reference [17] considers a group of N members, where each member $i = 1, \cdots, N$ is represented by a vector $x_i \in \mathbb{R}^p$ that consists of variables to be synchronized with the rest of the group. The communication structure between these members is described by a graph. The ith and jth members are called "neighbors" if they have access to the relative information $x_i - x_j$, in which case the ith and jth vertices of the graph are connected by an edge. To simplify the derivations [17] assigns an orientation to the graph by considering one of the vertices to be the positive end of the edge. The choice of orientation does not change the results since the information flow between neighbors are assumed to be bidirectional. Denoting by M the total number of edges, we recall from [83] that the $N \times M$ *incidence matrix* D of the graph is defined as:

$$d_{ik} = \begin{cases} +1 & \text{if } i\text{th vertex is the positive end of the } k\text{th edge} \\ -1 & \text{if } i\text{th vertex is the negative end of the } k\text{th edge} \\ 0 & \text{otherwise.} \end{cases} \tag{2.1}$$

Because the sum of its rows is zero, the rank of D is at most $N-1$. Indeed, the rank is $N-1$ when the graph is connected, that is when a path exists between every two distinct vertex, and less than $N-1$ otherwise. The columns of D are linearly independent when no cycles exist in the graph.

The objective is to develop coordination laws that are implementable with local information (the ith member can use the information $x_i - x_j$ if the jth member is a neighbor) and that guarantee the following two group behaviors:

B1) Each member achieves in the limit a common velocity vector $v(t) \in R^p$ prescribed for the group; that is $\lim_{t\to\infty} |\dot{x}_i - v(t)| = 0, \qquad i = 1, \cdots, N.$

B2) If ith and jth members are neighbors connected by link k, then the difference variable

$$z_k := \sum_{l=1}^{N} d_{lk} x_l = \begin{cases} x_i - x_j & \textit{if } i \textit{ is the positive end} \\ x_j - x_i & \textit{if } j \textit{ is the positive end} \end{cases} \tag{2.2}$$

converges to a prescribed compact set $\mathcal{A}_k \in R^p,\ k = 1, 2, ..., M$.

Examples of such target sets $\mathcal{A}_k$ include the origin if x_i's are variables that must reach an agreement within the group, or a sphere in $\mathbb{R}^p$ if x_i's are positions of vehicles that must maintain a prescribed distance. To achieve objectives B1-B2, [17] proposes a class of feedback laws of the form

$$\dot{x}_i = -\mathcal{H}_i \left\{ \sum_{k=1}^{M} d_{ik} \psi_k(z_k) \right\} + v(t) \quad i = 1, \cdots, N \tag{2.3}$$

where $\psi : \mathbb{R}^p \to \mathbb{R}^p$ is a multivariable nonlinearity to be designed, and $\mathcal{H}_i\{u_i\}$ denotes the output at time t of a static or dynamic block with input u_i. This block may represent the additional dynamics or nonlinearities inherent in the x_i-subsystem, or a filter introduced to improve performance or robustness of the design (5.18).

Note that the input of $\mathcal{H}_i$ in (2.3)

$$u_i := \sum_{k=1}^{M} d_{ik} \psi_k(z_k) \tag{2.4}$$

depends only on the neighbors of the ith member ($d_{ik} \neq 0$), thus, the feedback law (2.3) is implementable with local information. It follows from (2.2) that the concatenated vectors

$$x := [x_1^T \cdots x_N^T]^T \quad z := [z_1^T \cdots u_M^T]^T \tag{2.5}$$

satisfy

$$z = (D^T \otimes I_p)x \tag{2.6}$$

where I_p is the $p \times p$ identity matrix and " $\otimes$ " represents the Kronecker product, which means that z is constrained to lie in the range space $\mathcal{R}(D^T \otimes I_p)$. Therefore, if the columns of D are linearly dependent, i.e. if there are cycles in the graph, then z_k's are mutually dependent.

To obtain a block diagram representation for (2.3) we represent the output of $\mathcal{H}_i$ by the variable

$$y_i := \mathcal{H}_i(u_i), \tag{2.7}$$

and denote

$$y := [y_1^T \cdots y_N^T]^T \quad u := [u_1^T \cdots u_N^T]^T \quad \psi := [\psi_1^T \cdots \psi_M^T]^T. \tag{2.8}$$

Then, noting from (2.4) that

$$u = (D \otimes I_p)\psi, \tag{2.9}$$

and denoting by 1_p the p-dimensional column vector with all entries equal to 1 yields the right-hand side of (2.3) from the output of the summing junction in Figure 2.1.

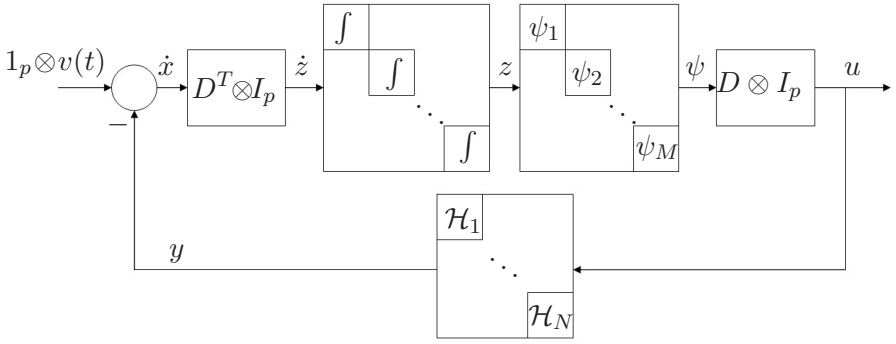

Figure 2.1: A block diagram representation for the interconnected system (2.3). The vectors x, y, z, u and ψ are as defined in (2.5) and (2.8), I_p is the $p \times p$ identity matrix, 1_p is the p-dimensional column vector with all entries equal to 1, and "$\otimes$" represents the Kronecker product.

2.2 Passivity-Based Design

Because post-multiplication by $D \otimes I_p$ and pre-multiplication by its transpose $D^T \otimes I_p$ preserve passivity properties, [17] proceeds with a passivity-based design of the filters $\mathcal{H}_i$, $i = 1, \cdots, N$, and nonlinearities ψ_k, $k = 1, \cdots, M$. Then objectives B1 and B2 are established with the help of Passivity Theorem [84, 85, 51] which guarantees the stability for the negative feedback interconnection of two passive systems.

The feedforward nonlinearities $\psi_k(z_k)$ are restricted to be of the form

$$\psi_k(z_k) = \nabla P_k(z_k) \tag{2.10}$$

where $P_k(z_k) : \mathbb{R}^p \to \mathbb{R}_{\geq 0}$ is a nonnegative C^2 function $P_k : \mathcal{G}_k \to \mathbb{R}_{\geq 0}$ defined on an open set $\mathcal{G}_k \subseteq R^p$ in which z_k is allowed to evolve. To steer z_k's to their target sets $A_k \subset \mathcal{G}_k$ while keeping them within G_k, we design the function $P_k(z_k)$ to grow unbounded as z_k approaches $\partial\mathcal{G}_k^\infty$ (boundary of $\mathcal{G}_k$), and let $P_k(z_k)$ and its gradient $\nabla P_k(z_k)$ vanish on the

set $\mathcal{A}_k$:

$$P_k(z_k) \to \infty \text{ as } z_k \to \partial\mathcal{G}_k^\infty \tag{2.11}$$

$$P_k(z_k) = 0 \Leftrightarrow z_k \in \mathcal{A}_k \tag{2.12}$$

$$\nabla P_k(z_k) = 0 \Leftrightarrow z_k \in \mathcal{A}_k. \tag{2.13}$$

In the feedback path, if $\mathcal{H}_i$ is a static block, it is restricted to be of the form

$$y_i = h_i(u_i) \tag{2.14}$$

where $h_i : \mathbb{R}^p \to \mathbb{R}^p$ is a locally Lipschitz function satisfying

$$u_i^T h_i(u_i) > 0 \quad \forall u_i \neq 0. \tag{2.15}$$

If $\mathcal{H}_i$ is a dynamic block of the form

$$\begin{aligned} \dot{\xi}_i &= f_i(\xi_i, u_i) \quad \xi_i \in \mathbb{R}^{n_i} \\ y_i &= h_i(\xi_i, u_i), \end{aligned} \tag{2.16}$$

it is assumed that $f_i(\cdot,\cdot)$ and $h_i(\cdot,\cdot)$ are locally Lipschitz functions such that $h_i(0,0) = 0$ and

$$f_i(0, u_i) = 0 \Rightarrow u_i = 0. \tag{2.17}$$

The main restriction on (2.16) is that it be strictly passive with a C^1, positive definite, radially unbounded storage function $S_i(\xi_i)$ satisfying

$$\dot{S}_i \leq -W_i(\xi_i) + u_i^T y_i \tag{2.18}$$

for some positive definite function $W_i(\cdot)$. Then using the storage functions

$$V_f(z) := \sum_{k=1}^{M} P_k(z_k) \quad \text{and} \quad V_b(\xi) := \sum_{i \in \mathcal{I}} S_i(\xi_i) \tag{2.19}$$

for the feedforward and feedback paths in Figure 2.1, respectively, [17] proves the stability of the interconnected system (2.1), (2.3) and (2.2) through the Passivity Theorem.

Theorem 2.1, [17]: *Consider the interconnected system (2.1), (2.2) and (2.3)*

represented with a block diagram in Figure 2.1. Suppose $v(t)$ is uniformly bounded and piecewise continuous, and ψ_k, $k = 1, \cdots, M$, and $\mathcal{H}_i$, $i = 1, \cdots N$, are designed as in (2.10)-(2.13) and (2.14)-(2.18). If the columns of D are linearly independent, then the set

$$\mathcal{A} = \{(z, \xi) | \xi = 0,\ z \in \mathcal{A}_1 \times \cdots \times \mathcal{A}_M \cap \mathcal{R}(D^T \otimes I_p)\} \tag{2.20}$$

is uniformly asymptotically stable with region of attraction

$$\mathcal{G} = \{(z, \xi) | \xi \in \mathbb{R}^{n_1} \times \cdots \times \mathbb{R}^{n_N},\ z \in \mathcal{G}_1 \times \cdots \times \mathcal{G}_M \cap \mathcal{R}(D^T \otimes I_p)\}. \tag{2.21}$$

When D has linearly dependent columns, $\mathcal{A}$ is uniformly locally asymptotically stable. Moreover, all trajectories $(z(t), \xi(t))$ starting in $\mathcal{G}$ converge to the set of equilibria

$$\mathcal{E} = \{(z, \xi) | \xi = 0,\ (D \otimes I_p)\psi(z) = 0 \text{ and } z \in \mathcal{R}(D^T \otimes I_p)\}. \tag{2.22}$$

□

Convergence to $\mathcal{A}$ means that the trajectories $x(t)$ converge to the set of points where the difference variables z_k belong to their target sets $\mathcal{A}_k$. It also implies that ξ and, thus, y in (2.7) tend to zero, which means that objectives B1 and B2 are indeed achieved.

2.3 Extension to Discrete-Time Agreement Protocols

Reference [17] also considers discrete-time agreement protocols of the form

$$x_i(n+1) - x_i(n) = -\mathcal{H}_i \left\{ \sum_{k=1}^{M} d_{ik} \psi_k(z_k(n)) \right\} + v(n), \tag{2.23}$$

where $n = 0, 1, 2, \cdots$ is the time index, and $\mathcal{H}_i$ is a discrete-time dynamic block or a static nonlinearity. The block diagram representation of this discrete-time model is as in Figure 2.1, with integral blocks replaced by summation blocks, and $\dot{x}$ and $\dot{z}$ replaced by, respectively,

$$\delta x = x(n+1) - x(n) \quad \text{and} \quad \delta z = z(n+1) - z(n). \tag{2.24}$$

Passivity of the feedforward path cannot be achieved in discrete-time because the phase lag of the summation block exceeds 90°. Indeed, with the further restriction

$$\nabla^2 P_k(z_k) \leq \gamma I \quad \forall z_k \in \mathbb{R}^p, \quad \gamma > 0 \tag{2.25}$$

it is shown in [17] that the storage function $V_f(z)$ in (2.19) satisfies

$$V_f(z(n+1)) - V_f(z(n)) \leq -u^T y + \frac{\gamma \lambda_N}{2} y^T y, \tag{2.26}$$

where λ_N denotes the largest eigenvalue of the graph Laplacian matrix DD^T. In particular, the second term on the right hand side of (2.26) quantifies the shortage of passivity.

To compensate for this shortage, [17] designs $\mathcal{H}_i$'s to achieve excess of passivity in the feedback path. If $\mathcal{H}_i$ is a static block $y_i = h_i(n, u_i)$, then we restrict it by

$$u_i^T y_i - \mu y_i^T y_i \geq w_i(u_i) \tag{2.27}$$

where $w_i(\cdot)$ is a positive definite function and the constant $\mu > 0$ quantifies the excess of passivity. Likewise, if $\mathcal{H}_i$ is a dynamic block of the form

$$\begin{aligned} \xi_i(n+1) &= f_i(\xi_i(n), u_i(n)) \quad \xi \in \mathbb{R}^{n_i} \\ y_i &= h_i(\xi_i, u_i) \end{aligned} \tag{2.28}$$

we assume that (2.17) holds and that there exists a positive definite and radially unbounded storage function $S_i(\xi_i)$ satisfying

$$S_i(\xi_i(n+1)) - S_i(\xi_i(n)) \leq -W_i(\xi) + u_i^T y_i - \mu y_i^T y_i \tag{2.29}$$

for some positive definite function $W_i(\cdot)$. We then guarantee stability of the feedback system by choosing

$$\mu \geq \frac{\gamma \lambda_N}{2}. \tag{2.30}$$

Theorem 2.2, [17]: *Consider members $i = 1, 2, ..., N$ interconnected as described by the graph representation (2.1), and let z_k, $k = 1, 2, ..., M$ denote the differences between the variables x_i of neighboring members as in (2.2). Let $P_k(z_k)$'s be C^2, positive definite, radially unbounded functions satisfying, (2.11)-(2.13) and (2.25). Suppose that $\mathcal{H}_i$'s are either dynamic blocks (2.28) satisfying (2.29)-(2.30), or static blocks $y_i = h_i(n, u_i)$ satisfying (2.27)-(2.30), or possibly a combination of such static and dynamic blocks. Then the feedback law (2.23) with $\psi_k(z_k) = \nabla P_k(z_k)$ achieves global asymptotic stability of the origin $(z, \xi) = 0$. In particular, if a path exists between the ith and jth vertices in the*

graph representation (2.1), then

$$x_i(n) - x_j(n) \to 0 \quad as \quad t \to \infty. \tag{2.31}$$

□

In addition to stabilizing feedback rules, the passivity approach in [17] constructs a Lurie-type Lyapunov function which can be used as a starting point for several robust redesigns.

CHAPTER 3
SYNCHRONIZED PATH FOLLOWING: A SAMPLED-DATA DESIGN

In this chapter, we extend the passivity-based design methodology to a class of sampled-data systems. To achieve this, we exploit the passivity property of the underlying continuous-time plant and make use of results from [34] on the preservation of dissipativity properties under sampling. Our main result establishes semiglobal asymptotic stability as the sampling period and a feedback gain are reduced. The sampled-data result is of particular importance because, in practice, the communication channel between the members of the group may necessitate a discrete-time implementation in the feedforward path, whereas in the feedback path the local controllers or internal dynamics of each member may be continuous-time.

In Section 3.1 we present the synchronized path-following problem in continuous-time interconnections. The main result (Theorem 3.1) in Section 3.2 proves semiglobal asymptotic stability by combining passivity tools with results from sampled-data systems [34]. We illustrate our design on a group of fully-actuated tugboats in Section 3.3.

3.1 Path Following Formulation

The objective in path-following problems is to design control laws that force the output of a system to follow a desired path, while obeying a dynamic assignment such as time, speed or acceleration along the path [86, 87, 88, 89]. In particular the formulation in [90] aims to develop control laws that force a system to follow a prescribed path, parameterized by a path variable θ, and that assign a desired speed to be achieved by $\dot{\theta}$ in the limit as $t \to \infty$. Synchronized path following is an extension of single vehicle path following to multi-vehicle case which aims at maneuvering the group while keeping them in a formation. To achieve this, individual paths are parametrized by a variable θ_i, and the paths are synchronized such that equal path parameters imply correct vehicle configuration. In this formulation, the vehicles only need to communicate their path variable and bandwidth demand is reduced.

We consider vehicles with the nonlinear dynamics

$$\dot{q}_i = f_i(q_i, u_i) \tag{3.1}$$

$$y_i = h_i(q_i) \tag{3.2}$$

and define the path error ξ_i as

$$\xi_i := \begin{bmatrix} y_i - y_d(\theta) \\ \dot{y}_i - \dot{y}_{di}(\theta) \end{bmatrix}, \tag{3.3}$$

where $y_d(\theta)$ is the desired path parametrized by θ. Reference [90] considers the path following problem for a single vehicle and designs a nonlinear controller of the norm:

$$\dot{\xi}_i = F_i(q_i)\xi_i - g_i(t, q_i, \theta)w_i, \tag{3.4}$$

$$\dot{\theta}_i = v(t) - w_i, \tag{3.5}$$

where the properties of F_i, g_i and w_i are detailed therein. The recent paper [35] extends the results in [90] to a group of vehicles having a coordinated path following motion using a feedback law of the form:

$$w_i = \mathcal{F}_i\{2\xi_i^T P_i g_i + u_i(\theta)\}, \tag{3.6}$$

where

$$u_i(\theta) = \sum_{k=1}^{M} d_{ik}\psi_k(\theta_i - \theta_k) \tag{3.7}$$

is the local information available to each vehicle. The block diagram structure of the path-following design is given in Figure 3.1.

3.2 Sampled-Data Design

We now study a sampled-data design in which θ_i (x_i in Section 2's notation) are updated in discrete-time as in (2.23), and the $\mathcal{H}_{2i}$ blocks consist of a combination of continuous- and discrete-time dynamics as depicted in Figure 3.2. The structure of $\mathcal{H}_{2i}$ is in part motivated by the formation design in [35] where each vehicle is driven by a path-following controller, and the path parameters θ_i are synchronized in discrete-time

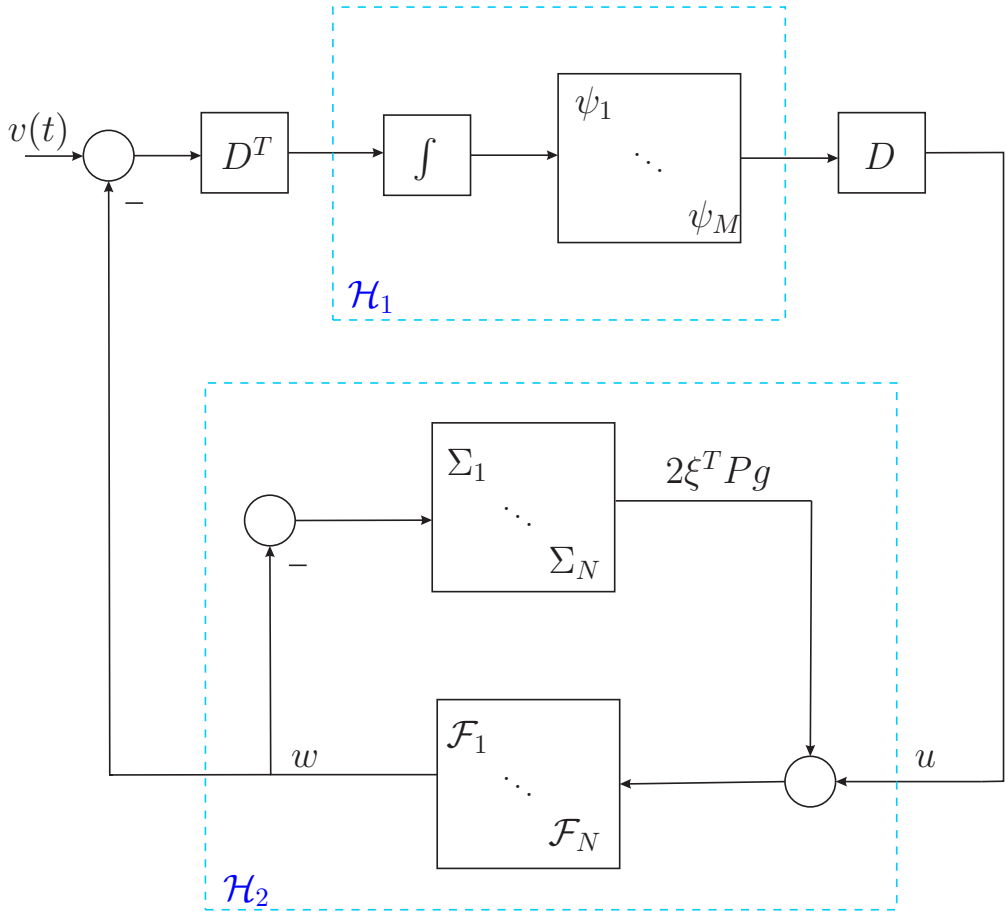

Figure 3.1: A block diagram representation of the synchronized path following controller structure. The feedforward block $\mathcal{H}_1$ achieves path variable synchronization while the feedback block $\mathcal{H}_2$ represents local path following controllers.

according to (2.23). The continuous-time vehicle dynamics play the role of the ξ_i-block in Figure 3.2, and η_i is a discrete-time correction term to achieve synchronization.

In this structure, Γ_i is a constant gain matrix, and the ξ_i-subsystem

$$\dot{\xi}_i = f_i(\xi_i, \eta_i) \tag{3.8}$$

$$\nu_i = h_i(\xi_i) \tag{3.9}$$

is such that $\xi_i \in \mathbb{R}^{n_i}$, and $f_i(\cdot,\cdot)$ and $h_i(\cdot)$ are locally Lipschitz functions such that $h_i(0) = 0$. We further assume that (3.8)-(3.9) is strictly passive with a C^2, positive definite storage function $S_i(\xi_i)$ such that

$$\dot{S}_i \leq -W(\xi_i) + \nu_i^T \eta_i \tag{3.10}$$

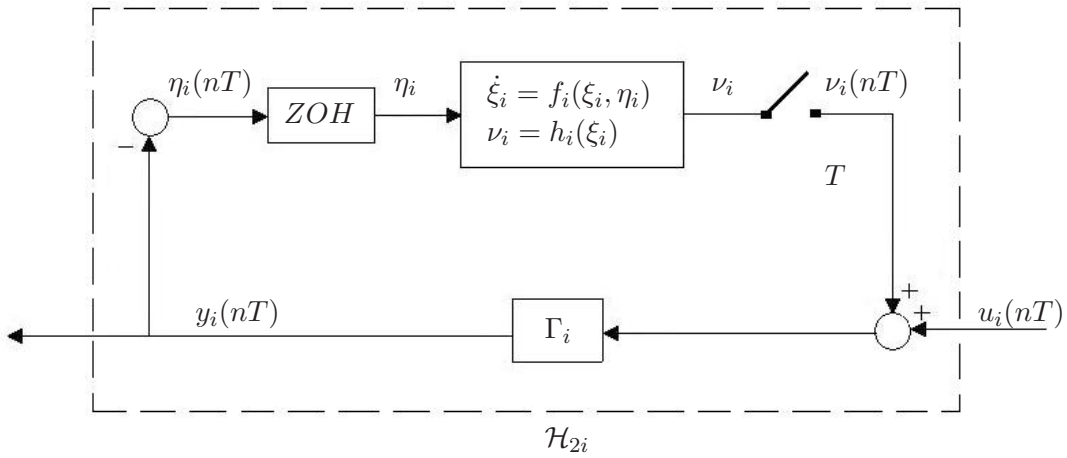

Figure 3.2: A block diagram representation of the sampled-data dynamic block $\mathcal{H}_i$ where Γ_i is a constant feedback gain matrix, ZOH stands for "Zero-Order-Hold" and T is the sampling period of ν_i.

for some positive definite function $W(\cdot)$.

3.2.1 Preservation of Passivity under Sampling

As a preparation for our main stability result, the following lemma characterizes to what extent the dissipation property (3.10) is preserved under sampling:

Lemma 3.1: *Suppose that $\mathcal{H}_i$ is a sampled-data dynamic block with the structure given in Figure 3.2. Assume that the continuous-time ξ_i-subsystem in (3.8)-(3.9) is passive with a C^2, positive definite storage function S_i satisfying (3.10). Then, given compact sets D_{ξ_i} and D_{η_i} there exist positive constants T_i^*, K_{1i}, K_{2i} such that for all sampling periods $T \in (0, T_i^*)$ and for all $(\xi_i(nT), \eta_i(nT)) \in D_{\xi_i} \times D_{\eta_i}$, the storage function S_i satisfies*

$$\begin{aligned}\frac{S_i(\xi_i(nT+T)) - S_i(\xi_i(nT))}{T} \leq & - W(\xi_i(nT)) + TK_{1i}\xi_i(nT)^T\xi_i(nT) \\ & + u_i(nT)^T y_i(nT) - (\frac{1}{\sigma_{\Gamma_i}} - TK_{2i}) y_i(nT)^T y_i(nT),\end{aligned} \tag{3.11}$$

where the design parameter σ_{Γ_i} denotes the largest singular value of Γ_i. □

Proof of Lemma 3.1: Since $\xi_i(nT)$ and $\eta_i(nT)$ lie in the compact sets D_{ξ_i} and D_{η_i}, respectively, we can find a pair of strictly positive numbers $(\Delta_{\xi_i}, \Delta_{\eta_i})$ such that $|\xi_i(nT)| \leq \Delta_{\xi_i}$, $|\eta_i(nT)| \leq \Delta_{\eta_i}$. Then, from [34, Prop. 3.4] and [34, Cor. 5.3], there exist $T_i^* > 0$ and positive constants K_{1i}, K_{2i} such that for all $T \in (0, T_i^*)$, $|\xi_i(nT)| \leq \Delta_{\xi_i}$ and

$|\eta_i(nT)| \leq \Delta_{\eta_i}$, we have:

$$\begin{aligned}\frac{S_i(\xi_i(nT+T)) - S_i(\xi_i(nT))}{T} \leq & - W(\xi_i(nT)) + \nu_i(nT)^T \eta_i(nT) \\ & + TK_{1i}\xi_i(nT)^T\xi_i(nT) + TK_{2i}\eta_i(nT)^T\eta_i(nT).\end{aligned} \tag{3.12}$$

For the given structure of the feedback path in Figure 3.2 we note that

$$\eta_i(nT) = -y_i(nT) \quad \text{and} \quad \nu_i(nT) = -u_i(nT) + \Gamma_i^{-1} y_i(nT). \tag{3.13}$$

To incorporate the feedback path from $u_i(nT)$ to $y_i(nT)$ with the storage function in (3.12), we substitute (3.13) into (3.12) and obtain:

$$\begin{aligned}\frac{S_i(\xi_i(nT+T)) - S_i(\xi_i(nT))}{T} \leq & - W(\xi_i(nT)) + TK_{1i}\xi_i(nT)^T\xi_i(nT) \\ & + u_i(nT)^T y_i(nT) - (\frac{1}{\sigma_{\Gamma_i}} - TK_{2i}) y_i(nT)^T y_i(nT),\end{aligned} \tag{3.14}$$

which completes the proof. □

3.2.2 Stability of the Interconnected System

To study the stability of the interconnected system (2.1), (2.2) and (2.23) we employ the storage functions

$$V_b(\xi) := \frac{1}{T}\sum_{i=1}^{N} S_i(\xi_i) \quad \text{and} \quad V_f(z) := \sum_{k=1}^{M} P_k(z_k), \tag{3.15}$$

for the feedback and feedforward paths, respectively, where P_k's are designed as in Section 3. We then prove that the origin $(z, \xi) = 0$ is semiglobally asymptotically stable in the sampling period T and in the feedback gain σ_Γ, which means that an arbitrarily large region of attraction for the origin can be achieved by making both T and σ_Γ sufficiently small.

Theorem 3.1: *Consider members $i = 1, 2, ..., N$ interconnected as described by the graph representation (2.1), and let z_k, $k = 1, 2, ..., M$ denote the differences between the variables θ_i of neighboring members as in (2.2). Let $P_k(z_k)$'s be designed as C^2, positive definite, radially unbounded functions satisfying (2.11)-(2.13) and (2.25). Suppose that*

$\mathcal{H}_i$'s are sampled-data dynamic blocks as in Figure 3.2, and satisfy (3.10) and the following two assumptions:

A1. *$W(\xi_i)$ in (3.10) is lower bounded by $W(\xi_i) \geq C|\xi_i|^2$ for some $C > 0$,*

A2. *ξ_i-subsystems, $i = 1, \cdots, N$ are input-to-state stable (ISS) from η_i to ξ_i,* i.e. *there exist class $-\mathcal{KL}$ and class $-\mathcal{K}$ functions $\beta(\cdot,\cdot)$ and $\alpha(\cdot)$, respectively, such that*

$$|\xi_i(t)| \leq \beta(|\xi_i(t_0)|, t - t_0) + \alpha(\sup_{t_0 \leq \tau \leq t} |\eta_i(\tau)|). \tag{3.16}$$

Then given compact sets $\mathcal{D}_z$ and $\mathcal{D}_\xi$ there exist positive constants $\overline{T}$ and $\bar{\sigma}$ such that for all sampling periods $T < \overline{T}$ and $\sigma_{\max}(\Gamma) < \bar{\sigma}$, the feedback law (2.23) with $\psi_k(z_k) = \nabla P_k(z_k)$ achieves asymptotic stability of the origin $(z, \xi) = 0$ with a region of attraction that includes $\mathcal{D}_z \times \mathcal{D}_\xi$. □

Proof of Theorem 3.1: For the interconnected system we take the Lyapunov function $V(z, \xi) = V_f(z) + V_b(\xi)$, and let $\mathcal{S} =: \mathcal{S}_z \times \mathcal{S}_\xi$ denote a level set of $V(z, \xi)$, such that $\mathcal{S} \supset \mathcal{D}_z \times \mathcal{D}_\xi$. We note from Figure 3.2, (2.9) and (3.9) that

$$\eta_i(nT) = -\Gamma_i(u_i(nT) + \nu_i(nT)) = -\Gamma_i\Big(\sum_{k=1}^{M} d_{ik}\psi_k(z_k(nT)) + h_i(\xi_i(nT))\Big). \tag{3.17}$$

Therefore, given a compact set $\mathcal{S}$ and a positive number σ^*, there exists a compact set $\mathcal{D}_\eta$ such that

$$\sigma_{\max}(\Gamma) < \sigma^* \quad \text{and} \quad (z(nT), \xi(nT)) \in \mathcal{S} \Longrightarrow \eta(nT) \in \mathcal{D}_\eta. \tag{3.18}$$

We then apply Lemma 1 with $(\xi(nT), \eta(nT)) \in (\mathcal{S}_\xi \times \mathcal{D}_\eta)$, and obtain T^*, K_1 and K_2, such that, from (3.14) and (3.15), for all sampling periods $T < T^*$,

$$\begin{aligned} V_b(\xi(nT + T)) - V_b(\xi(nT)) \;\leq\; & -\sum_{i=1}^{N} \Big\{ W(\xi_i(nT)) - TK_1\xi_i(nT)^T\xi_i(nT) \Big\} \\ & + \; u(nT)^T y(nT) - \Big(\frac{1}{\sigma_{\max}(\Gamma)} - TK_2\Big) y(nT)^T y(nT). \end{aligned} \tag{3.19}$$

We then define

$$\frac{1}{\sigma^{**}} := TK_2 + \frac{\gamma\lambda_N}{2}, \tag{3.20}$$

and note that for all $T < T^*$ and $\sigma_{\max}(\Gamma) < \sigma^{**}$, (3.19) and ***A1*** yields

$$\begin{aligned} V_b(\xi(nT+T)) - V_b(\xi(nT)) \leq & - (C - TK_1)\xi(nT)^T\xi(nT) + u(nT)^T y(nT) \\ & - \kappa y(nT)^T y(nT), \end{aligned} \tag{3.21}$$

where $\kappa > \frac{\gamma\lambda_N}{2}$ from (3.20). To make the first term in the right hand side of (3.21) negative definite, we define

$$T^{**} := \frac{C}{K_1}, \tag{3.22}$$

and then note that for all sampling periods $T < T^{**}$,

$$(C - TK_1)\xi(nT)^T\xi(nT) > 0 \quad \forall \xi(nT) \in S_\xi - \{0\}. \tag{3.23}$$

Finally, we define

$$\bar{\sigma} =: \min\{\sigma^*, \sigma^{**}\} \quad \text{and} \quad \overline{T} := \min\{T^*, T^{**}\}, \tag{3.24}$$

and conclude from (2.26), (3.21) and (3.23) that for all $\sigma_{\max}(\Gamma) < \bar{\sigma}$, $T < \overline{T}$, and $\xi(nT) \in S_\xi - \{0\}$, $V(z,\xi)$ satisfies:

$$\begin{aligned} V(z(nT+T),\xi(nT+T)) - V(z(nT),\xi(nT)) \leq & - (C - TK_1)\xi(nT)^T\xi(nT) \\ & - (\kappa - \frac{\gamma\lambda_N}{2})y(nT)^T y(nT) < 0, \end{aligned} \tag{3.25}$$

which implies that the trajectories $(z(nT), \xi(nT))$ are bounded and stay in $\mathcal{S}$. It further follows from standard arguments that there exists a $class - \mathcal{K}$ function α_1 such that for all $(z(0), \xi(0)) \in S$,

$$|z(nT), \xi(nT)| \leq \alpha_1(|z(0), \xi(0)|). \tag{3.26}$$

To study the behavior of the trajectories between the sampling points we first note from (3.17) that

$$|\eta(nT)| \leq ||\Gamma||\Big(L_h|\xi(nT)| + ||D \otimes I_p||L_\psi|z(nT)|\Big) =: \alpha_2(|\xi(nT), z(nT)|), \tag{3.27}$$

where L_h and L_ψ are Lipschitz constants of $h(\cdot)$ and $\psi(\cdot)$ in S, respectively, and α_2 is a $class - \mathcal{K}$ function by construction. From the ISS property in (3.16), we obtain for all

$t \in [nT, nT+T]$

$$|\xi(t)| \leq \beta(|\xi(nT)|, 0) + \alpha(\alpha_2(|\xi(nT), z(nT)|)) =: \alpha_3(|\xi(nT), z(nT)|), \tag{3.28}$$

where α_3 is also a $class-\mathcal{K}$ function. Next, because $z(t)$ is constant between the sampling points, we can combine (3.28) and (3.26) and obtain another $class-\mathcal{K}$ function α_4 such that for all $(z(0), \xi(0)) \in \mathcal{S}$,

$$|z(t), \xi(t)| \leq \alpha_4(|z(0), \xi(0)|), \tag{3.29}$$

which proves stability of the origin $(z, \xi) = 0$.

Finally, to conclude asymptotic stability with a region of attraction containing $\mathcal{S}$ we note from (3.25) that as $n \to \infty$, $\xi(nT) \to 0$ and $y(nT) \to 0$, hence, $u(nT) \to 0$ from (3.13) and the property $h_i(0) = 0$. It then follows from similar arguments in the proof of Theorem 1 that $u(nT) \to 0$ implies $\psi_k(z_k) = \nabla P_k(z_k) \to 0$, $k = 1, \cdots, M$, which proves that $z(nT) \to 0$. We thus conclude, using (3.28), that $(z(t), \xi(t)) \to 0$ as $t \to \infty$. □

3.3 Example

We consider a group of fully actuated tugboats previously studied in [35]. The body-fixed equations of motion for vessel $i = 1, ..., N$ are given as [91]:

$$\dot{\pi}_i = R(\phi_i)\rho_i \tag{3.30}$$

$$M_i\dot{\rho}_i + C_i(\rho_i)\rho_i + D_i(\rho_i)\rho_i = \tau_i, \tag{3.31}$$

where $\pi_i = [x_i, y_i, \phi_i]$ is the earth-fixed position vector, (x_i, y_i) is the position on the ocean surface and ϕ_i is the heading angle (yaw), and $\rho_i = [u_i, v_i, r_i]$ is the body fixed velocity vector. The model matrices M_i, C_i, and D_i denote inertia, Coriolis plus centrifugal, and damping, respectively. The vector τ_i consists of generalized control forces and moments, and R_i is the rotation matrix between the body and Earth coordinate frame, and satisfies $R(\phi_i)^T R(\phi_i) = I$, $||R(\phi_i)|| = 1$, $\forall i$, and $(d/dt)R(\phi_i) = R(\phi_i)S\phi_i$ where $S = -S^T$ is skew-symmetric.

For each vessel we assign an individual path where the desired path for vessel i is given by $\pi_{di}(\theta_i) = [x_{di}(\theta_i), y_{di}(\theta_i), \phi_{di}(\theta_i)]$. By construction, the paths are scaled appropriately such that when the vessels are in the desired formation configuration the path

variables are synchronized. The tangent vector along the path is chosen as the x-axis of the moving frame that is $T(\theta_i) = [x_{di}^{\theta_i}(\theta_i), y_{di}^{\theta_i}(\theta_i)]$. The desired heading can then be computed as the angle of the tangent vector in the Earth frame

$$\phi_d(\theta_i) = \arctan\Big(\frac{y_{di}^{\theta_i}(\theta_i)}{x_{di}^{\theta_i}(\theta_i)}\Big). \tag{3.32}$$

Then, given a path $\pi_{di}(\theta_i)$ and a speed assignment $v(t)$ the design in [35] gives a path-following control law for (3.30)-(3.31). A backstepping design [51] for each ship model gives the static part of the control signal

$$\tau_i = -z_{1i} - K_i z_{2i} + D(\rho_i)\rho_i + C_i(\rho_i)\rho_i + M_i(\delta_{1i} + \alpha_{1i}^{\theta_i} v) \tag{3.33}$$

where $K_{di} = K_{di}^T > 0$, α_{1i} is a virtual control determined by the backstepping procedure, and $\dot{\alpha}_{1i} = \delta_{1i} + \alpha_{1i}^{\theta_i}\dot{\theta}$. Then the resulting closed-loop system is given by (3.4)-(3.5) where, for $K_{pi} = K_{pi}^T > 0$,

$$F_i(\rho_i) := \begin{bmatrix} -K_{pi} - r_i S & I \\ -M_i^{-1} & -M_i^{-1}(K_{di} + D_i(\rho_i) + c_i(\rho_i)) \end{bmatrix} \tag{3.34}$$

$$g(\pi_i, \theta_i, t) := \begin{bmatrix} R(\phi_i)\pi_{di}^{\theta_i}(\theta_i) \\ \alpha_{1i}^{\theta_i}(\eta_i, \theta_i, t) \end{bmatrix}. \tag{3.35}$$

In our simulation we assign each vessel a circular path given by

$$\pi_{di}(\theta_i) = \begin{bmatrix} r\cos(\theta_i/r) \\ r\sin(\theta_i/r) \\ \arctan\Big(\frac{x_d^{\theta_i}(\theta_i)}{y_d^{\theta_i}(\theta_i)}\Big) \end{bmatrix}, \tag{3.36}$$

where r is the radius. Each path is scaled such that equal speed assignments imply that, after synchronization of all path parameters has occurred, the vessels will move along their respective paths parallel to each other as in Figure 3.3. We update the path parameters θ_i (x_i in Section 2's notation) in discrete time as in (2.23), and let the path following controllers in (3.4)-(3.5) run in a sampled-data fashion implemented as in Figure 3.2 with two sets of parameters $T = 5,\ \sigma(\bar{\Gamma}) = 2$ and $T = 0.5,\ \sigma = 0.2$. The simulation results in Figures 3.4 and 3.5 verify the result in Theorem 3.1 that we achieve convergence by reducing the sampling period T and the feedback gain Γ.

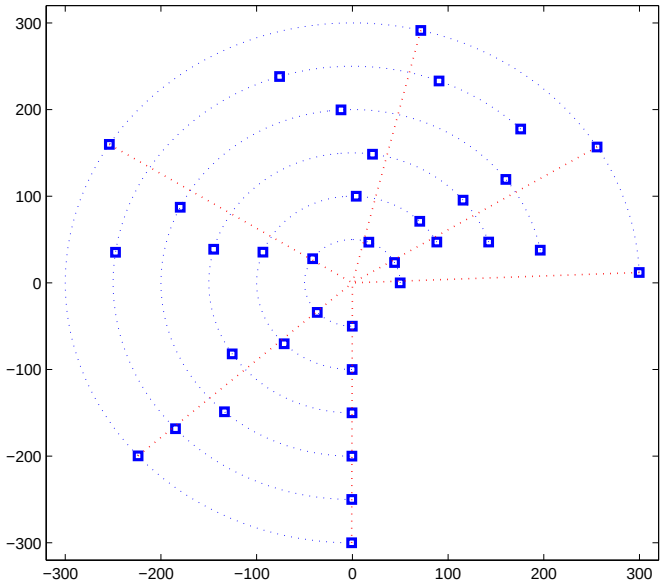

Figure 3.3: Snapshots of synchronized path following by 6-tugboats on a concentric circular path. Blue squares represent the vessels, while the red dotted line is the radial direction of vessel 6. When the path parameters θ_i are synchronized, the vessels align at the same radial direction, which means that they all have same heading angle as desired.

3.4 Summary

We have extended the passivity-based design methodology to a class of sampled-data systems. The sampled-data result is of particular importance because, in practice, the communication channel between the members of the group may necessitate a discrete-time implementation in the feedforward path, whereas in the feedback path the local controllers or internal dynamics of each member may be continuous-time. Our result showed that in such sampled-data implementations the size of the region of attraction is determined by the sampling period and the feedback gain. Our result is also applicable to time-varying sampling periods that are upper bounded by $\bar{T}$.

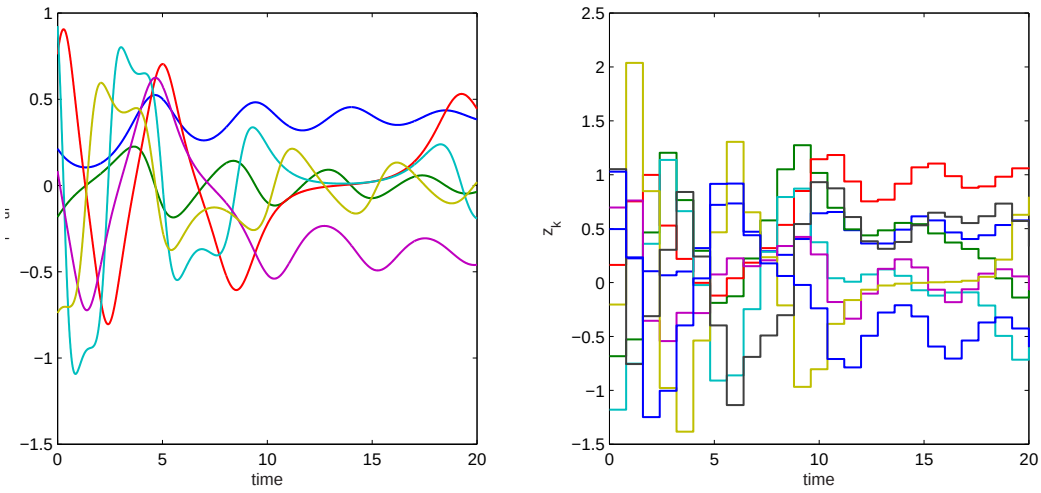

Figure 3.4: Simulation result for 6-tugboat sampled-data path following with $T = 0.8$ and $\bar{\sigma}(\Gamma) = 2$. Path following error ξ and path variable error z_k do not converge to the origin.

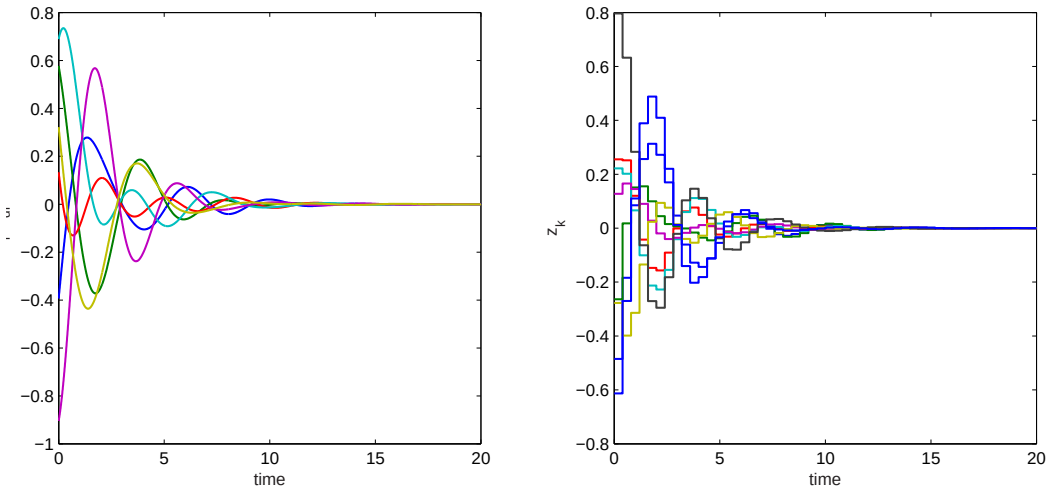

Figure 3.5: Simulation result for 6-tugboat sampled-data path following with reduced parameters $T = 0.3$ and $\bar{\sigma}(\Gamma) = 0.2$. As predicted by Theorem 3.1, path following error ξ and path variable error z_k converge to the origin.

CHAPTER 4
GRADIENT CLIMBING IN FORMATION VIA EXTREMUM-SEEKING AND PASSIVITY-BASED COORDINATION RULES

In this chapter we take a discrete-time, optimization based extremum seeking approach for gradient climbing. In our design, to achieve a successful gradient climbing by a group of vehicles while keeping a formation, the leader has a parameterized velocity that facilitates an adaptive reconstruction of this information by the followers. We show that if there is sufficient time-scale separation between the fast dither and slow gradient motions of the leader vehicle, the followers only respond to the gradient motion, and filter out the dither component.

Section 4.1 presents the extremum-seeking motion of the leader vehicle, and proves convergence to the maxima of the field. Section 4.2 combines leader vehicle's extremum seeking motion with the followers' coordination laws, and proves the stability of the formation while locating the extrema of the field distribution. Section 4.3 gives a design example that illustrates the proposed scheme. Section 4.4 discusses alternative optimization methods that can be utilized for additional robustness and power-efficiency, and gives a simulation example.

4.1 Reference Velocity Assignment via Extremum Seeking

In this section, we present the extremum seeking scheme performed by the leader. The detailed analysis of the motion of the group will be pursued in Section 4.2. Our goal in extremum-seeking based gradient climbing is to search for and move towards the maximum of a field distribution with an unknown functional form. We follow the optimization approach, where the vehicle has access only to the scalar field measurements, and constructs the approximate gradient and Hessian information of the field by finite-difference methods to compute a Newton direction. The motion controller on the vehicle then assigns the appropriate velocity that drives the vehicle along the computed Newton direction. It is important to note that, in this scheme, the vehicle locates the maxima without position measurements.

We first review the basic optimization tools that are instrumental in our extremum seeking design. We assume the field has a spatial distribution characterized by a twice

continuously differentiable function[1] $F(x) : \mathbb{R}^2 \to \mathbb{R}$ that has a unique[2] maximum at $x = x^*$. Because only field measurements are available to the leader, we employ one-sided finite-difference gradient, G_k,

$$\nabla F(x_k) \approx G_k[i] := \frac{F(x_k + h_k e_i) - F(x_k)}{h_k} \tag{4.1}$$

and Hessian, H_k,

$$\begin{aligned}\nabla^2 F(x_k) \approx H_k[i,j] := & \frac{1}{h_k^2}\Big[F(x_k) + F(x_k + h_k e_i + h_k e_j) \\ & - F(x_k + h_k e_i) - F(x_k + h_k e_j)\Big]\end{aligned} \tag{4.2}$$

approximations, where h_k denotes the finite-difference "dither" size, and e_i is the i^{th} unit vector. Alternative methods such as line-search, Quasi-Newton (BFGS) [92], and Simultaneous Perturbation Stochastic Approximations (SPSA) [93, 94] are briefly discussed in Section 4.4. For an easier implementation, steepest descent (only three field measurements) may be preferable over Newton's Method; however, it is slower and does not provide a concrete convergence proof with nonvanishing step-size. We denote by $\mathcal{N}(\bar{x}, a)$ the ball of radius a centered at $\bar{x}$, *i.e* $\mathcal{N}(\bar{x}, a) := \{x : ||x - \bar{x}|| \leq a\}$. The lemma below states that for sufficiently small dither size h_k, and for small initial error $||x_0 - x^*||$, finite-difference based Newton's Method locally converges to an $\mathcal{O}(h)$-neighborhood of x^*. The proof follows from standard arguments in unconstrained optimization theory, and is given in Appendix A for completeness.

Lemma 4.1: *Let $F(x) : \mathbb{R}^2 \to \mathbb{R}$ be twice continuously differentiable in an open convex set $D \in \mathbb{R}^2$. Assume there exists a unique $x^* \in \mathbb{R}^2$, $r > 0$ and $\beta > 0$ such that $\mathcal{N}(x^*, r) \in D$, $\nabla F(x^*) = 0$, $\nabla^2 F(x^*)^{-1}$ exists with $||\nabla^2 F(x^*)^{-1}|| \leq \beta$, $\nabla F(x)$ and $\nabla^2 F(x)$ are Lipschitz continuous. Then there exist $\epsilon > 0$ and $\bar{h} > 0$, such that for all initial conditions $x_0 \in \mathcal{N}(x^*, \epsilon)$, and dither size $h_k < \bar{h}$ the sequence $\{x_k\}_{k=0}^{k=\infty}$ generated by*

$$x_{k+1} = x_k + H_k^{-1} G_k, \quad k = 0, 1, \cdots \tag{4.3}$$

where G_k and H_k are as in (4.1)-(4.2) converges to an $\mathcal{O}(\bar{h})$ neighborhood of x^* q-linearly.

[1] We restrict our attention to $\mathbb{R}^2$, however, our results can be extended to $\mathbb{R}^3$ as well by employing appropriate finite-difference approximations.

[2] If the function $F(x)$ has multiple maxima, then our results can be modified to prove regional convergence to the local maximum.

□

We next introduce a Newton's Method-based extremum seeking scheme that the leader performs to locate the maximum of the field. Following the passivity framework introduced in [17], we consider agents with the dynamic model

$$\dot{x}_i = h_i(\xi_i, u_i) + v(t), \quad i = 1, \cdots, N \tag{4.4}$$

$$\dot{\xi}_i = f_i(\xi_i, u_i) \tag{4.5}$$

where $x_i \in \mathbb{R}^2$ and $\xi \in \mathbb{R}^2$ denote the position and internal dynamics of each vehicle, respectively, u_i is an external feedback law as in (2.4), and $v(t)$ is the reference group velocity. An example of such a model is the fully-actuated point mass

$$\ddot{x}_i = f_i \tag{4.6}$$

where $x_i \in \mathbb{R}^2$ is the position of each mass and $f_i \in \mathbb{R}^2$ is the input force. Indeed, the internal feedback law

$$f_i = -K_i(\dot{x}_i(t) - v(t)) + \dot{v}(t) + u_i, \qquad K_i > 0 \tag{4.7}$$

and the change of variables $\xi_i = \dot{x}_i - v(t)$ bring (4.6) into the form

$$\dot{x}_i = \xi_i + v(t) \tag{4.8}$$

$$\dot{\xi}_i = -K_i\xi_i + u_i \tag{4.9}$$

which is as in (4.4)-(4.5). The leader, say the first vehicle, does not receive external feedback from other members of the group, hence $u_1 = 0$. Without loss of generality we assume $\xi_1(0) = 0$, *i.e.* the vehicle is initially at rest, which yields the leader dynamics

$$\dot{x} = v_1(t). \tag{4.10}$$

Note that if $\xi_1(0) \neq 0$, we can apply the velocity input $\tilde{v} = -h(\xi_1, 0) + v_1(t)$, and recover (4.10).

We use Newton's Method to determine the next position for the vehicle, and set the velocity $v_1(t)$ to steer the vehicle to that position. In the kth extremum-seeking iteration,

the leader first moves in $[1,\ 0]$, $[-1,\ 1]$, and $[0,\ -1]$ directions rapidly to take samples of the field $F(x)$, and computes the approximate gradient G_k and the Hessian H_k as in (4.1)-(4.2), and then moves in the approximate Newton direction $d_k = H_k^{-1}G_k$, and arrives at $x_{k+1} = x_k + d_k$ as illustrated in Figure 4.1.

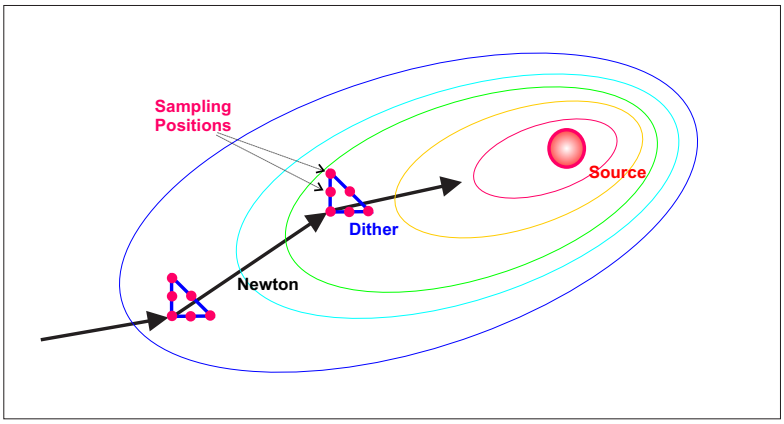

Figure 4.1: Gradient climbing by extremum seeking. Arrows represent the slow Newton motion, while triangular paths represent the fast dither motion with the samples taken at positions marked by dots.

To prepare for an adaptive velocity estimation by the followers as in [95], we need to have the velocity vector in a parameterized form. For each motion segment we let the velocity have a fixed sinusoidal amplitude profile, with endpoints at zero, and change its direction between successive segments. This sinusoidal amplitude profile allows us to construct the velocity information of the vehicle adaptively using the results in [95]. There are other techniques to assign the velocity vector in discrete-time extremum seeking, e.g. set-point stabilization, [96, 97], but they require position measurements, and do not provide a parameterized reference velocity, hence are not suitable for the adaptive estimation design in this chapter.

We let $v_{[i,j]}$ and v_N denote the dither velocity in $[i,j]$ direction, $[i,j] \in \Big\{[1,0],[-1,1],$ $[0,-1]\Big\}$, and the Newton velocity in d_k direction, respectively, and τ denote the duration of each dither motion segment, and T be that of the Newton motion. Therefore one iteration of the extremum seeking scheme takes $\Delta := 3\tau + T$ seconds. During each extremum seeking

iteration, the vehicle switches its velocity as

$$\dot{x}_1 = v_1(t) := \begin{cases} v_{[1,0]}(t), & \text{if } t_k \le t < t_k + \tau, \\ v_{[-1,1]}(t), & \text{if } t_k + \tau \le t < t_k + 2\tau, \\ v_{[0,-1]}(t), & \text{if } t_k + 2\tau \le t < t_k + 3\tau, \\ v_N(t), & \text{if } t_k + 3\tau \le t < t_{k+1}, \end{cases} \tag{4.11}$$

where $t_k := k\Delta$, $k = 0, 1, 2, \cdots$, and $v_{[1,0]}$, $v_{[-1,1]}$, $v_{[0,-1]}$ and v_N are defined as in (4.12)-(4.15):

$$v_{[1,0]}(t) := \frac{2h_k}{\tau}\begin{bmatrix} 1 \\ 0 \end{bmatrix}\Big(1 - \cos(\frac{2\pi}{\tau}(t - t_k))\Big) \tag{4.12}$$

$$v_{[-1,1]}(t) := \frac{2h_k}{\tau}\begin{bmatrix} -1 \\ 1 \end{bmatrix}\Big(1 - \cos(\frac{2\pi}{\tau}(t - t_k - \tau))\Big) \tag{4.13}$$

$$v_{[0,-1]}(t) := \frac{2h_k}{\tau}\begin{bmatrix} 0 \\ -1 \end{bmatrix}\Big(1 - \cos(\frac{2\pi}{\tau}(t - t_k - 2\tau))\Big) \tag{4.14}$$

$$v_N(t) := \frac{d_k}{T}\Big(1 - \cos(\frac{2\pi}{T}(t - t_k - 3\tau))\Big). \tag{4.15}$$

We note that the velocity input $v_1(t)$ in (4.11) and its derivative $\dot{v}_1(t)$ are continuous, and $(v_1(t), \dot{v}_1(t))|_{t\in\{t_k+n\tau,\ t_{k+1}\}} = (0, 0),\ n = 0, 1, 2, 3$. In our design, however, the choice of velocity profiles are not restricted to (4.12)-(4.15). Other continuous velocity profiles that vanish at $t \in \{t_k + n\tau,\ t_{k+1}\},\ n = 0, 1, 2, 3$, along with their derivatives, are also applicable. The velocities in (4.12)-(4.15), when switched according to (4.11), achieve one iteration of extremum-seeing motion by driving the vehicle first to the appropriate dither positions and then to the next "Newton" position x_{k+1}. Theorem 1 below proves that our extremum seeking scheme converges to an $\mathcal{O}(\bar{h})$ neighborhood of the maximum x^*, when $h_k \le \bar{h}$ is as in Lemma 1, and $||x(0) - x^*||$ is sufficiently small.

Theorem 4.1: *Let the field distribution $F(x)$ be twice continuously differentiable with a unique maximum at position $x = x^* \in \mathbb{R}^2$. Suppose the assumptions in Lemma 1 hold and $\bar{h}$ be as defined therein. Then the Newton-based extremum seeking scheme applied to the vehicle model in (4.11) with velocity profiles (4.12)-(4.15) drives the vehicle to the $O(\bar{h})$ neighborhood of x^*, provided that $h_k \le \bar{h}$ and $||x(0) - x^*||$ is sufficiently small.* □

Proof of Theorem 4.1: We show that the velocity profiles given in (4.11) first drive the vehicle in the appropriate dither directions, and then along the Newton direction.

Consider $v_{[1,0]}$ which drives the vehicle in horizontal position, i.e. along the vector $[1,0]$. At time t_k, let the position of vehicle be x_k, then at time $t_k + \tau/2$ its position is:

$$\begin{aligned} x(t_k+\frac{\tau}{2}) &= x(t_k)+\int_{t_k}^{t_k+\tau/2} v_{[1,0]}(t)dt \\ &= x(t_k)+\frac{2h_k}{\tau}\begin{bmatrix}1\\0\end{bmatrix}\int_{t_k}^{t_k+\tau/2}(1-\cos(\frac{2\pi}{\tau}(t-t_k)))dt \\ &= x(t_k)+\frac{2h_k}{\tau}\begin{bmatrix}1\\0\end{bmatrix}\Big[t-\frac{\tau}{2\pi}\sin(\frac{2\pi}{\tau}(t-t_k))\Big]\Big|_{t_k}^{t_k+\tau/2} \\ &= x(t_k)+h_k\begin{bmatrix}1\\0\end{bmatrix} = \begin{bmatrix}x^1(t_k)+h_k\\ x^2(t_k)\end{bmatrix}. \end{aligned} \tag{4.16}$$

Likewise,

$$\begin{aligned} x(t_k+\tau) &= x(t_k+\tau/2)+\int_{t_k+\tau/2}^{t_k+\tau} v_{[1,0]}(t)dt \\ &= x(t_k+\tau/2)+h_k\begin{bmatrix}1\\0\end{bmatrix} = \begin{bmatrix}x^1(t_k)+2h_k\\ x^2(t_k)\end{bmatrix}. \end{aligned} \tag{4.17}$$

Similar calculations show that $v_{[-1,1]}$ and $v_{[0,-1]}$ achieve the desired dither motions as well. Note that after the third dither motion $v_{[0,-1]}$ the vehicle will be back at position $x(t_k+3\tau) = x(t_k) = x_k$. Then, applying the velocity v_N after this point for T seconds drives the vehicle to

$$\begin{aligned} x(t_k+\Delta) &= x(t_k)+d_k\frac{1}{T}\int_{t_k+3\tau}^{t_k+3\tau+T}(1-\cos(\frac{2\pi}{T}(t-t_k-3\tau)))dt \\ &= x(t_k)+d_k = x(t_{k+1}). \end{aligned} \tag{4.18}$$

Therefore, by appropriately switching the velocities defined in (4.11) the vehicle visits all dither positions and then moves to the next Newton position. The convergence result follows from Lemma 1. □

We have shown that using the switching strategy in (4.11) with the velocity $v_1(t)$ parameterized as in (4.12)-(4.15), the leader locates the extrema of the field. We next study the motion of the group while achieving the gradient climbing.

4.2 Gradient Climbing in Formation

We now study the behavior of the group in response to the leader's extremum seeking motion. We combine the passivity-based group coordination laws with the leader's extremum seeking motion, and study the formation dynamics with respect to the leader's dynamics. Note that the followers do not have the knowledge of the velocity $v_1(t)$ which changes after each iteration of extremum seeking. Our adaptive design aims to estimate the gradient motion component of $v_1(t)$ while filtering out the fast dither motion component, so that the followers do not respond to the dither. We first review a recent result [95] on adaptive reference velocity estimation by the followers.

4.2.1 Leader Following: Adaptive Velocity Estimation

In reference [95], the situation where only the leader has the velocity information is studied, and an adaptive velocity estimation scheme that reconstructs this information is developed. This study assumes that the velocity of the leader $v_1(t) \in \mathbb{R}^p$ is parameterized as

$$v_1(t) = \sum_{j=1}^{r} \phi^j(t)\theta^j \tag{4.19}$$

where $\phi^j(t),\ j = 1, \ldots, r$ are uniformly bounded scalar base functions available to each agent and θ^j are column vectors available only to the leader. Other vehicles estimate the unknown θ^j by $\hat{\theta}^j$, and construct reference velocity estimate $\hat{v}_i(t)$ through the formula

$$\hat{v}_i(t) = \sum_{j=1}^{r} \phi^j(t)\hat{\theta}^j = (\Phi(t)^T \otimes I_p)\hat{\theta}_i \quad i = 2, \cdots, N, \tag{4.20}$$

where $\Phi(t) := [\phi^1(t), \cdots, \phi^r(t)]^T$ and $\hat{\theta}_i := [(\hat{\theta}_i^1)^T, \cdots, (\hat{\theta}_i^r)^T]^T$, and the parameter $\hat{\theta}^j$ is obtained by the update law

$$\dot{\hat{\theta}}_i = \Lambda_i(\Phi(t) \otimes I_p)u_i \tag{4.21}$$

in which $\Lambda_i = \Lambda_i^T > 0$ is the adaptive gain matrix and u_i is as in (2.4). It is proven in [95] that the convergence result in Theorem 2 is recovered by modifying (4.4) as

$$\dot{x}_1 = h_1(\xi_1, 0) + v_1(t) \tag{4.22}$$

$$\dot{x}_i = h_i(\xi_i, u_i) + \hat{v}_i(t) \quad i = 2, \cdots, N. \tag{4.23}$$

4.2.2 Group Dynamics During the Dither Motion

During the dither motion, the followers can turn off the velocity adaptation scheme so that they do not respond to the dither. Even if the adaptation is not turned off, an averaging analysis in [51, Section 10.6] shows that when τ is small the followers detect only the slow Newton motion, and average out the dither component. Indeed, from (4.11), the average of the leader's dynamics within one extremum seeking iteration are

$$v_{1,av} := \frac{1}{\Delta}\int_{t_k}^{t_k+\Delta} v_1(t)dt = \frac{1}{\Delta}d_k, \tag{4.24}$$

and $\Delta \approx T$ if τ is small. Then, it follows from [95, Theorem 2] that using the adaptation law in (4.20), (4.21), (4.23) the formation is reconstructed within each extremum-seeking iteration if T is sufficiently large.

4.2.3 Two-Time-Scale Behavior During the Newton Motion

We now reveal the two-time-scale behavior in the group motion induced by a large T, and show that the convergence to the desired formation is achieved in the fast time scale, while the Newton motion is performed in the slow time-scale. We consider only the Newton motion segment of the group in kth extremum seeking iteration, and let $w := 1/T$, $\bar{t} := t - t_k - 3\tau,\ \bar{t} \in [0,\ T]$. Then in the slow time-scale $\sigma := w\bar{t}$, the leader dynamics in (4.10) become

$$\frac{dx_1}{d\sigma} = d_k\phi(\sigma), \quad \sigma \in [0,1]. \tag{4.25}$$

where $\phi(\sigma) := (1-\cos(2\pi\sigma))$. We let the base function available to the followers be $\Phi(\sigma) := w\phi(\sigma) = w(1-\cos(2\pi\sigma)) \in \mathbb{R}$ from (4.15), and assume a uniform adaptation gain $\Lambda_i = \lambda I_2,\ i = 2, ..., N$, in (4.21) where $\lambda > 0$ is constant. We then denote by $\tilde{\theta}_i$ the error variable

$$\tilde{\theta}_i = \hat{\theta}_i - \theta \quad i = 2, \cdots, N$$

and note from (4.21) that

$$\dot{\tilde{\theta}}_i = \lambda\Phi(\sigma)u_i \quad i = 2, \cdots, N \tag{4.26}$$

For consistency with (2.5) and (2.8), we set $\tilde{\theta}_1 \equiv (0,0)^T$, and define

$$\tilde{\theta} = [\tilde{\theta}_1^T, \tilde{\theta}_2^T, \cdots, \tilde{\theta}_N^T].$$

Using (2.6), (4.5), (4.21), and the property

$$(D^T \otimes I_p)(1_N \otimes v(t)) = 0 \tag{4.27}$$

which results from the fact that the sum of the rows of D is zero, the fast $(z, \xi, \tilde{\theta})$ dynamics are obtained as:

$$\begin{aligned} w\frac{dz}{d\sigma} &= (D^T \otimes I_2)(h(\xi, u) + w\phi(\sigma)\tilde{\theta}), && (4.28)\\ w\frac{d\xi}{d\sigma} &= f(\xi, u) + (D \otimes I_2)\psi(z), && (4.29)\\ \frac{1}{\lambda}\frac{d\tilde{\theta}}{d\sigma} &= \phi(\sigma)(D \otimes I_2)\psi(z). && (4.30) \end{aligned}$$

Note that w acts also as a regular perturbation parameter in z-dynamics. When w is small, the reference velocity is slowly time-varying, hence the mismatch between $v_1(t)$ and $\hat{v}(t)$ become less effective on the formation dynamics. We pick the adaptation gain $\lambda = \mathcal{O}(T) = \mathcal{O}(1/w)$, so that $\tilde{\theta}$ has fast dynamics as well. System (4.25), (4.28)-(4.30) is then in a singularly perturbed form. Letting $w \to 0$ yields the quasi-steady state equations:

$$\begin{aligned} 0 &= (D^T \otimes I_2)h(\bar{\xi}, u), && (4.31)\\ 0 &= f(\bar{\xi}, u) + (D \otimes I_2)\psi(\bar{z}), && (4.32)\\ 0 &= \phi(\sigma)(D \otimes I_2)\psi(\bar{z}). && (4.33) \end{aligned}$$

We note that (4.33) is time-varying, and average $\phi(\sigma)$ over $\sigma \in [0, 1]$ to obtain

$$\begin{aligned} 0 &= \int_0^1 \phi(\sigma)d\sigma(D \otimes I_2)\psi(\bar{z}) && (4.34)\\ &= \int_0^1 (1 - \cos(2\pi\sigma))d\sigma(D \otimes I_2)\psi(\bar{z}) && (4.35)\\ &= (D \otimes I_2)\psi(\bar{z}) && (4.36) \end{aligned}$$

which implies $\bar{z}_k \in \mathcal{A}_k$, and $u = 0$ from (5.26). We then conclude $f(\bar{\xi}, u) = 0$ from (4.32), which implies $\bar{\xi} = 0$ from $u = 0$ and (2.17), and satisfies (4.31). Then the quasi-steady states are $(\bar{z}, \bar{\xi}) = (\bar{z}_k \in \mathcal{A}_k, 0)$.

4.2.4 Rescaling the Formation Dynamics

Smaller T allows faster convergence to the field maxima, but it reduces the time-scale separation between leader motion and the rest of the dynamics. We now circumvent this trade-off by rescaling the design parameters, and accelerating the formation dynamics uniformly. We consider the model in (4.8)-(4.9), which yields

$$\dot{z} = (D^T \otimes I_2)\xi + w\phi(t)(D^T \otimes I_2)\tilde{\theta} \tag{4.37}$$

$$\dot{\xi} = -K\xi + (D \otimes I_2)\psi(z) \tag{4.38}$$

$$\dot{\tilde{\theta}} = \lambda w\phi(t)(D \otimes I_2)\psi(z), \tag{4.39}$$

where $K = K^T := \text{diag}(K_i) > 0$. When T is reduced to $\epsilon T,\ \epsilon < 1$, we define the new variable $\hat{\xi} := \epsilon\xi$ and rescale K, $\psi(\cdot)$ and λ as $K \to K/\epsilon,\ \psi(\cdot) \to \psi(\cdot)/\epsilon^2,\ \lambda \to \epsilon^2\lambda$. Then, in the new variables the system (4.37)-(4.39) takes the form

$$\epsilon\dot{z} = (D^T \otimes I_2)\hat{\xi} + w\phi(t)(D^T \otimes I_2)\tilde{\theta} \tag{4.40}$$

$$\epsilon\dot{\hat{\xi}} = -K\hat{\xi} + (D \otimes I_2)\psi(z) \tag{4.41}$$

$$\epsilon\dot{\tilde{\theta}} = \lambda w\phi(t)(D \otimes I_2)\psi(z), \tag{4.42}$$

which evolves in a faster time-scale than (4.37)-(4.39).

4.3 Design Example

We study the gradient climbing of four vehicles, modelled as fully-actuated point-masses

$$\ddot{x}_i = f_i, \quad i = 1, 2, 3, 4 \tag{4.43}$$

where $x_i \in \mathbb{R}^2$ is the position of each mass and $f_i \in \mathbb{R}^2$is the input force.

To stabilize a rhombus formation with the relative distances $|z_1| = |x_1 - x_2| = \sqrt{3}$, and $|z_k| = |x_i - x_j| = 1$, $k = 2, \cdots, 6$, $i, j = 1, \cdots, 4$, $i \neq j$, we design $\mathcal{A}_1$ to be a circle with radius $r = \sqrt{3}$, $\mathcal{A}_k$ to be the unit circle, $k = 2, \cdots, 6$, $\mathcal{G}_k$ to be $\mathbb{R}^2 \setminus \{0\}$, and let the potential functions be of the form

$$P_1(z_1) = \int_{\sqrt{3}}^{|z_k|} \sigma_1(s)ds, \quad P_k(z_k) = \int_1^{|z_k|} \sigma_k(s)ds \tag{4.44}$$

where $\sigma_k : \mathbb{R}_{>0} \to \mathbb{R}$ is a C^1, strictly increasing function such that

$$\sigma_1(\sqrt{3}) = 0, \sigma_k(1) = 0, \lim_{s\to\infty} \sigma_k(s) = \infty, \lim_{s\to 0} \sigma_k(s) = -\infty \tag{4.45}$$

and such that, as $|z_k| \to \infty$, $P_k(z_k) \to \infty$ in (4.44). Then $P_k(z_k)$ satisfies (2.10)-(2.13), and the feedback law (2.4) with the interaction forces

$$\psi_k(z_k) = \nabla P_k(z_k) = \sigma_k(|z_k|)\frac{1}{|z_k|}z_k \qquad z_k \neq 0 \tag{4.46}$$

guarantees asymptotic stability of the desired formation from Theorem 2. For the simulations we take $\sigma_1(s) = \ln(s/\sqrt{3})$ and $\sigma_k(s) = \ln(s)$.

We let the field distribution be

$$F(x, y) = e^{-0.1e^{0.1x}(1.1x-5)^2 - 0.2e^{0.1y}(0.8y-4)^2},$$

which has a global maximum at $x = [4.5, 5]$. We fix $\Delta = 20$ and $h_k = 0.05$, and pick $\tau = 0.5$sec and $T = 18.5$sec for the first simulation. We run the system (4.22)-(4.23), where the leader determines its velocity by extremum seeking as in (4.11) and (4.12)-(4.15). Figure 4.2 shows that after an initial transient, vehicles follow the leader's Newton motion in a rhombus formation, and average out the fast dither perturbations, while the leader locates the maxima of the field. In the second simulation, we perform the dither motion at a slower speed with $\tau = 4$sec, $T = 8$sec. In this case, the vehicles in Figure 4.3 fail to average out the dither motion, and follow a jittering trajectory.

4.4 Discussion and Summary

We considered a combined gradient climbing and formation design, and showed that if there is sufficient time-scale separation between the slow gradient motion and the fast dither motion, the formation dynamics act as a boundary-layer system relative to the leader vehicle dynamics. The leader's velocity is introduced in a parameterized form so that an adaptive reconstruction can be pursued by the rest of the vehicles to follow the gradient motion while averaging out dither motion.

Our Newton's Method based extremum seeking scheme proves local convergence to the maxima. Most of the global convergence results in the literature require a line search that adaptively finds a step size for each iteration. In a line search, however, additional function evaluations (field measurements) are required, which limits the applicability to

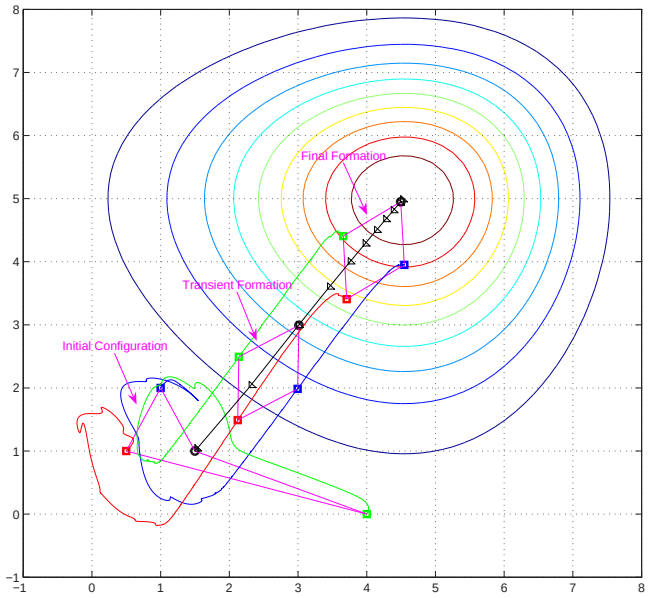

Figure 4.2: Gradient climbing by Newton-based extremum seeking. $T = 18.5$, $\tau = 0.5$, $h_k = 0.05$. **Black line represents the leader's trajectory, while red, blue, and green are the followers'. After an initial transient vehicles follow the leader's Newton motion in a rhombus formation, and average out the fast dither perturbations.**

our problem. The Quasi-Newton method BFGS recursively updates the Hessian approximation and, hence, reduces the number of measurements. A local *practical* convergence proof for BFGS can be pursued using the tools in [98] which rely on the exact knowledge of $\nabla F(x)$, and global versions can be achieved via line search.

To address the effect of noise in the field and in the measurements, stochastic gradient approximations can be pursued, such as those in [99, 100]. To minimize the energy consumption of the leader caused by the dither motion we can employ the simultaneous perturbation stochastic approximation method [93], which reduces the number of dither directions and measurements required for the gradient approximation. The SPSA algorithm presented in [93, 94] recursively estimates the minimizer of a function $f(x) : \mathcal{D} \subseteq \mathbb{R}^n \to \mathbb{R}$ based on its noisy measurements through the formula

$$x_{k+1} = x_k - \alpha_k \frac{y_k^+ - y_k^-}{2c_k} d_k \tag{4.47}$$

where both a_k and c_k are positive scalars, $d_k \in \mathbb{R}^n$ is a random direction vector, y_k^+ and

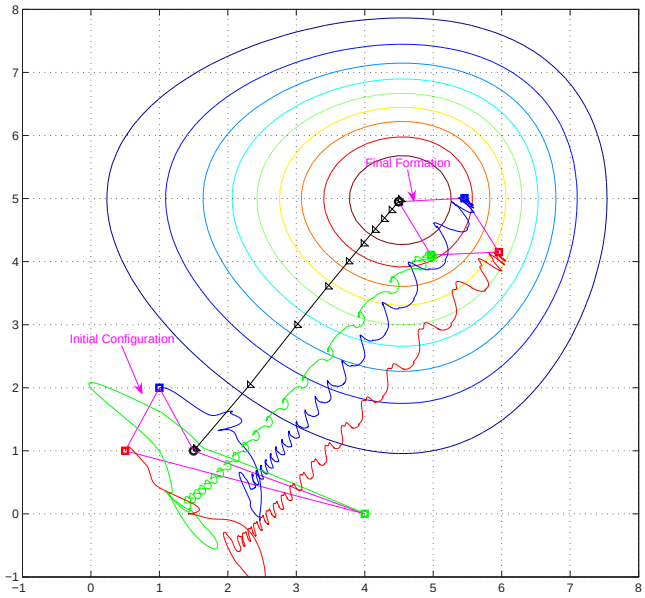

Figure 4.3: Gradient climbing by Newton-based extremum seeking. $T = 8$, $\tau = 4$, $h_k = 0.05$. **Black line represents the leader's trajectory, while red, blue, and green are the followers'. The vehicles fail to average out the dither motion, and follow a jittering trajectory.**

y_k^- are the noisy measurements of $f(x)$ defined by:

$$y_k^+ = f(x_k + c_k d_k) + e_k^+ \tag{4.48}$$

$$y_k^- = f(x_k - c_k d_k) + e_k^+ \tag{4.49}$$

where e_k^+ and e_k^- are additive measurement errors. The restriction on the random direction d_k is that it is a vector of n mutually independent mean-zero random variables with bounded inverse moments (which precludes d_k being uniformly or normally distributed), e.g. symmetrically Bernoulli distributed $d_k[i] = \pm 1,\ i = 1, 2, ..., n$. Note that the SPSA algorithm requires only two measurements of the function $f(x)$ regardless of the problem dimension n. This provides a substantial computational advantage in large scale optimization problems.

Below we present two simulation studies that show the the performance of an SPSA based extremum seeking scheme. We add a Gaussian noise with zero mean to the field measurements and let the search vehicle estimate the gradient of the field using random dithers as in (4.48)-(4.49), and move along that estimated gradient. As shown in Figures 4.4 and 4.5, the vehicle successfully locates the maximum of the field using local

measurements. As a next step, we plan to combine the search vehicle's SPSA-based extremum seeking motion with a group coordination algorithm as in Section 4.2, and pursue a detailed analysis of stability and performance.

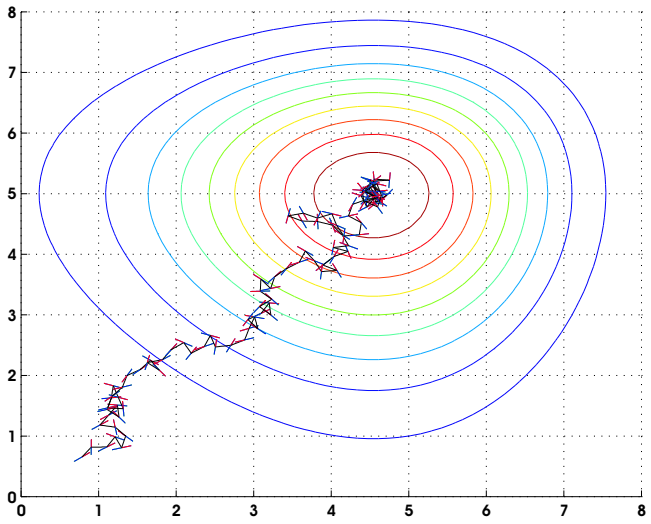

Figure 4.4: Extremum seeking by SPSA using random search directions. Blue lines represent the gradient motion, whereas red lines represent the random dither motion.

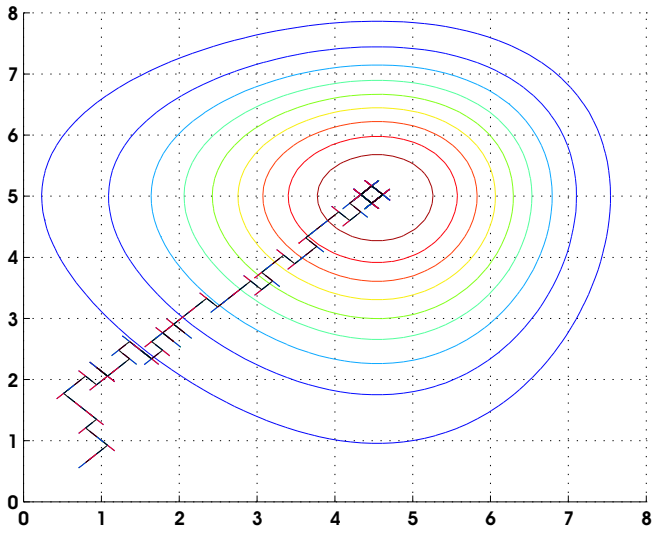

Figure 4.5: Extremum seeking by SPSA using symmetrically Bernoulli distributed search direction $d_k[i] = \pm 1,\ i = 1, 2$. Blue lines represent the gradient motion, whereas red lines represent the random dither motion.

CHAPTER 5
AREA AGGREGATION AND TIME-SCALE MODELING FOR SPARSE NONLINEAR NETWORKS

Model reduction and aggregation are of key importance for simulation and analysis of large-scale systems, such as molecular dynamics, large swarms of robotic vehicles, and animal aggregations. In this chapter we study a nonlinear network which exhibits a clustered interconnection structure where coherent areas are characterized by internally dense and externally sparse interconnections, and develop a model reduction technique that exploits a time-scale separation property induced by this clustered interconnection structure. We show that the densely connected nodes in these areas synchronize in the fast time-scale, and behave as aggregate nodes that dominate the slow dynamics of the network. We first derive a singular perturbation model which makes this time-scale separation explicit and, next, prove the validity of the reduced-model approximation on the infinite time interval.

In Section 5.2, the dynamic network model and the agreement problem are introduced. Section 5.3 motivates our area aggregation and time-scale separation study on a formation control example. Section 5.4 characterizes the sparse interconnection structure of the network. Section 5.5 introduces slow and fast variables that reveal the time-scale separation in the network. Section 5.6 obtains the singular perturbation model of the network and presents the main result in Theorem 5.1.

5.1 Problem Statement

We study a network of N nodes, where each node $i = 1, \cdots, N$ is represented by a variable[3] $x_i \in \mathbb{R}$ which is to be synchronized with the rest of the group while asymptotically achieving a reference group velocity $v(t)$:

$$\lim_{t\to\infty} |x_i(t) - x_j(t)| = 0, \qquad i, j = 1, \cdots, N, \tag{5.1}$$

$$\lim_{t\to\infty} |\dot{x}_i - v(t)| = 0, \qquad i = 1, \cdots, N. \tag{5.2}$$

[3]Our results can be extended to higher dimensions, i.e. $x_i \in \mathbb{R}^n$, $n > 1$, using Kronecker algebra; however, for the clarity of the analysis we take x_i to be a scalar.

As shown in [17], objectives (5.1)-(5.2) are achieved by the distributed feedback law:

$$\dot{x}_i = -\sum_{k=1}^{M} d_{ik}\psi_k(\zeta_k) + v(t) \quad i = 1, \cdots, N, \tag{5.3}$$

where ζ_k denotes the difference variable

$$\zeta_k := \sum_{l=1}^{N} d_{lk}x_l = \begin{cases} x_i - x_j & \text{if } i \text{ is the positive end} \\ x_j - x_i & \text{if } j \text{ is the positive end} \end{cases} \tag{5.4}$$

and $\psi_k(\zeta_k)$ is a sector nonlinearity; that is,

$$\psi_k(\zeta_k)\zeta_k > 0 \ \ \forall \zeta_k \neq 0. \tag{5.5}$$

In our analysis, we further assume that $\psi_k(\zeta_k)$ is uniformly monotone; i.e. there exists $\epsilon > 0$ such that,

$$\psi_k' := \frac{d\psi_k(\zeta_k)}{d\zeta_k} \geq \epsilon \quad \forall \zeta_k \in \mathbb{R}. \tag{5.6}$$

In this chapter we study the effect of the network topology on the transient behavior of (5.3). Our first contribution is to prove that a topology that exhibits areas of internally dense and externally sparse interconnections leads to a two-time-scale behavior where nodes within the same area reach an agreement in the fast time-scale. The areas then act as aggregate nodes which reach an agreement in the slow time-scale (see the example in Section 5.2). Our second contribution is to exploit this two-time-scale behavior to obtain a reduced-order model in which areas are represented as aggregate nodes. Reduced models are of central importance in large-scale systems, such as power networks, because they enable numerically tractable simulations that predict system performance under changing parameters and operating conditions [20, 21, 22].

When the network is linear, our result can be interpreted based on a clustering of the eigenvalues in the system matrix. Indeed, when ψ_k is identity, equation (5.3) can be rewritten as $\dot{x} = -Lx + v(t)$ where $L := DD^T$ is the graph Laplacian. If the graph exhibits r disconnected areas L contains r eigenvalues at zero [83]. If, instead of being disconnected, these areas are sparsely connected, then L will exhibit a cluster of r eigenvalues close to zero (including one exactly at zero) which suggests the existence of r slow modes that dominate the long term behavior of the network. In this chapter we make this time-scale

separation property explicit with a novel change of variables that brings the nonlinear system (5.3) to a standard singularly perturbed form.

5.2 Motivating Example: Synchronized Path Following

We consider a 48-vehicle formation, where each vehicle is steered by a path following controller [90], and the path parameters x_i are synchronized as in (5.3). The communication structure in our example is given in Figure 5.1, and exhibits three areas of internally dense and externally sparse interconnections. Such a clustered interconnection structure may be preferable because much simpler and efficient protocols can be used for routing and broadcasting within a cluster. In a dense cluster, the data obtained by sensors are similar, and therefore the aggregation and reduction of the data would be performed locally by the cluster-heads to save energy. To show that this structure indeed leads to two

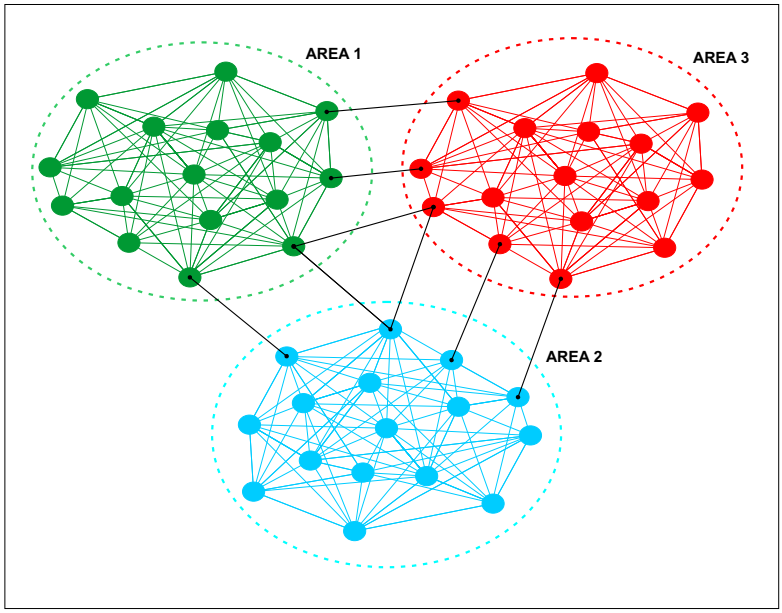

Figure 5.1: 48-node network partitioned into 3 areas. Green: Area 1, Blue: Area 2, Red: Area 3.

time scales, we perform simulations in which each vehicle synchronizes its variable x_i with other vehicles using (5.3), while the path-following controller drives the vehicles to follow the path:

$$p_i^h = x_i \tag{5.7}$$

$$p_i^v = 2i + \sin(x_i), \quad i = 1, ..., 48, \tag{5.8}$$

where p_i^h and p_i^v denote the horizontal and vertical components of i^{th} path, respectively. The explicit forms of the vehicle dynamics and the path-following controllers can be derived using the results in [90], and are omitted due to space limitation.

In the simulations, we pick $\psi_k(\zeta_k) = \zeta_k^3$ in (5.3) and choose the reference velocity for x to be $v(t) = 0.3$. At time $t = 0$ all vehicles are randomly placed in the plane as shown in Figure 5.2. After a short initial transient, however, the vehicles cluster into the areas identified in Figure 5.1, which afterwards behave as aggregate nodes and synchronize in a slower time scale.

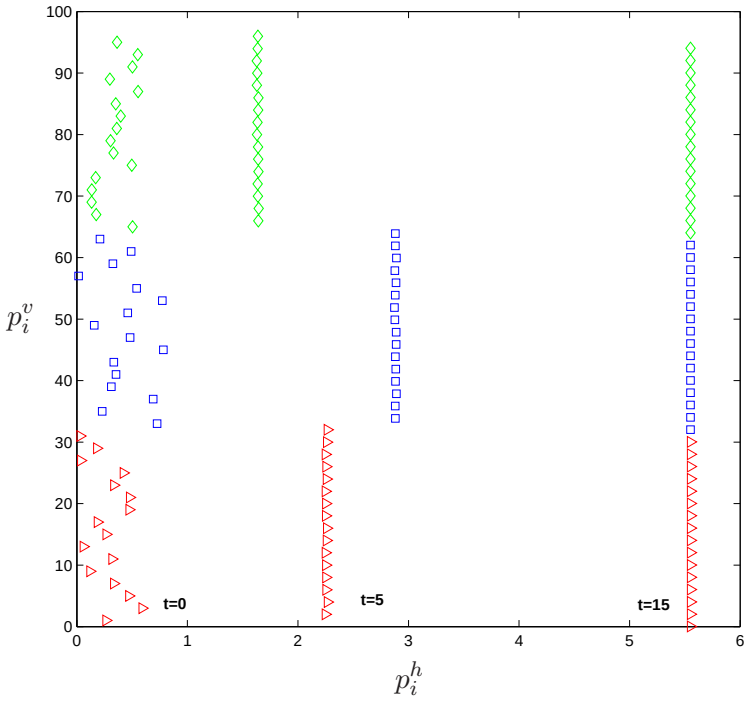

Figure 5.2: Trajectories of the 48-vehicle formation. The vehicles cluster into coherent areas that synchronize with each other in the slow time scale. Diamonds represent vehicles in area 1 of Figure 5.1, while squares and triangles are the vehicles in areas 2 and 3, respectively.

5.3 Characterization of Sparsity

In this section we partition the network into r areas that have internally dense and externally sparse links as, for example, in Figure 5.1. We characterize the sparse interconnection by a node parameter d and an area parameter δ. The node parameter d

characterizes the sparsity of the external links with respect to individual nodes, whereas δ characterizes the sparsity with respect to the areas. As we shall see in the subsequent sections, both parameters must be sufficiently small for the accuracy of the reduced model. In particular, δ is a singular perturbation parameter, and d is a regular perturbation parameter that, when small, guarantees a weak coupling between fast and slow variables.

5.3.1 Node parameter d

The i^{th} node in area α has dense internal links and sparse external links if

$$\frac{c^E_{\alpha i}}{c^I_{\alpha i}} \ll 1, \tag{5.9}$$

where $c^E_{\alpha i}$ and $c^I_{\alpha i}$ denote the number of external and internal links of node i in area α, respectively. We note that, from the sparsity point of view, the least favorable nodes are those with the sparsest internal links c^I and densest external links c^E, where

$$c^I := \min_{\alpha,i}\{c^I_{\alpha i}\} \quad \text{and} \quad c^E := \max_{\alpha,i}\{c^E_{\alpha i}\}. \tag{5.10}$$

For sparsity, we want even the worst node to have more internal links than the external links, that is the node parameter

$$d := \frac{c^E}{c^I} \tag{5.11}$$

must be small.

5.3.2 Area parameter δ

The α^{th} area has sparse external and dense internal links if

$$\frac{\gamma^E_\alpha}{\gamma^I_\alpha} \ll 1, \tag{5.12}$$

where γ^E_α and γ^I_α denote the total number of external and internal links in area α, respectively. The least favorable areas are those with the sparsest internal links γ^I and the densest external links γ^E, where

$$\gamma^I := \min_{\alpha}\{\gamma^I_\alpha\} \quad \text{and} \quad \gamma^E := \max_{\alpha}\{\gamma^E_\alpha\}. \tag{5.13}$$

We note that γ^I is, in general, compatible with mc^I, that is

$$\gamma^I = \mathcal{O}(mc^I), \tag{5.14}$$

where $m := \min_\alpha\{m_\alpha\}$, and m_α is the number of nodes in area α. Our goal is to find a partitioning in which even the worst area has more internal links than external links; that is, the area parameter

$$\delta := \frac{\gamma^E}{mc^I} \tag{5.15}$$

must be small. We denote the total number of internal and external links in the network by Γ^I and Γ^E, respectively, and note that $\Gamma^I + \Gamma^E = M$.

Algorithms for identifying coherent areas in large power networks are given in [20], [101] and [102]. In particular, [101] studies partitioning algorithms that achieve minimal d and δ.

5.4 Slow and Fast Variables

As a preparation for the time-scale separation result in Section 5.5, we now introduce a set of fast and slow variables. To this end, we note from (5.4) that the concatenated vectors

$$x := [x_1 \cdots x_N]^T \quad \zeta := [\zeta_1 \cdots \zeta_M]^T \tag{5.16}$$

satisfy

$$\zeta = D^T x, \tag{5.17}$$

and rewrite (5.3) as

$$\dot{x} = -D\Psi(D^T x) + 1_N v(t), \tag{5.18}$$

where 1_N denotes the N-vector of 1's, and

$$\Psi(\zeta) := [\psi_1(\zeta_1),\ \psi_2(\zeta_2),\ \ldots,\ \psi_M(\zeta_M)]^T. \tag{5.19}$$

We suppose that the N-node network has been decomposed into r internally dense,

sparsely connected areas, with each area having m_α nodes, $\alpha = 1, 2, ...r$, and that the vector x is ordered such that

$$x = \left[(x^1)^T \ (x^2)^T \ \dots \ (x^r)^T\right]^T, \tag{5.20}$$

where

$$x^\alpha := [x_1^\alpha \ x_2^\alpha \ \cdots \ x_{m_\alpha}^\alpha]^T \tag{5.21}$$

denotes the nodes in area α.

We model the slow motion of the areas with the aggregate variable

$$y_\alpha := \sum_{i=1}^{m_\alpha} \frac{x_i^\alpha}{m_\alpha} = \frac{1}{m_\alpha} u_\alpha^T x^\alpha, \tag{5.22}$$

where u_α is an m_α-vector of 1's, that is,

$$u_\alpha = [1 \ 1 \ \cdots \ 1]^T. \tag{5.23}$$

Denoting by y the r-vector whose α^{th} entry is y_α, we rewrite (5.22) as

$$y = M_a^{-1} U^T x, \tag{5.24}$$

where

$$M_a := \text{diag}(m_1, m_2, \cdots, m_r), \tag{5.25}$$

and

$$U := \text{diag}(u_1, u_2, \cdots, u_r) \tag{5.26}$$

is an $N \times r$ block-diagonal matrix whose diagonal $m_\alpha \times 1$ blocks are the u_α vectors in (5.23).

We next define the fast variable z_α, which represents the differences between the nodes within the same area,

$$z_\alpha = Q_\alpha x^\alpha, \tag{5.27}$$

where z_α is an $(m_\alpha - 1)$-vector, and Q_α is an $(m_\alpha - 1) \times m_\alpha$ matrix selected as:

$$Q_\alpha \;\; = \;\; \Delta(m_\alpha), \tag{5.28}$$

where

$$\Delta(n) \;\; := \;\; \begin{bmatrix} -1+(n-1)\nu & 1-\nu & -\nu & \dots & -\nu \\ -1+(n-1)\nu & -\nu & 1-\nu & \dots & -\nu \\ \vdots & \vdots & \dots & \ddots & -\nu \\ -1+(n-1)\nu & -\nu & \dots & -\nu & 1-\nu \end{bmatrix}, \tag{5.29}$$

$$\tag{5.30}$$

$$\nu \;\; := \;\; \frac{n-\sqrt{n}}{n(n-1)} < 1, \;\; n = 2, 3, \dots \tag{5.31}$$

Because Q_α has orthonormal rows that are each orthogonal to 1_{m_α}, we conclude that

$$Q_\alpha 1_{m_\alpha} = 0 \qquad Q_\alpha Q_\alpha^T = I_{m_\alpha - 1}, \tag{5.32}$$

where $I_{m_\alpha - 1}$ denotes the $(m_\alpha - 1) \times (m_\alpha - 1)$ identity matrix. We note that $z_\alpha = 0$ when $x^\alpha = \mathcal{R}(1_{m_\alpha})$ (when all nodes in area α are synchronized). Next, denoting by z the $(N - r)$-vector

$$z = [z_1^T \;\; z_2^T \;\; \cdots \;\; z_r^T]^T, \tag{5.33}$$

we obtain

$$z = Qx, \tag{5.34}$$

where Q is an $(N - r) \times N$ block diagonal matrix $Q := \text{diag}(Q_1, Q_2, ..., Q_r)$. We note that Q also has the property $QQ^T = I_{N-r}$, and that the range space of U lies in the nullspace of Q, i.e $Qw = 0, \forall w \in \mathcal{R}(U)$.

The inverse of the transformation (5.24)-(5.34) is then explicitly obtained as

$$x = Uy + Q^T z. \tag{5.35}$$

With the change of variables (5.24)-(5.34), from (5.18) and (5.35), the dynamic equations

governing the (y, z) system are

$$\dot{y} = -M_a^{-1}U^T D\Psi(D^T U y + D^T Q^T z) + M_a^{-1}U^T 1_N v(t) \quad (5.36)$$

$$\dot{z} = -QD\Psi(D^T U y + D^T Q^T z). \quad (5.37)$$

Because $1_N \in \mathcal{R}(U) \Rightarrow Q1_N = 0$, the velocity vector $v(t)$ does not appear in the z-dynamics.

When $\Psi(\cdot)$ is the identity function and $v(t) = 0$ we recover the linear network studied in [50]:

$$\dot{x} = -Lx, \quad (5.38)$$

where $L := DD^T$ is the graph Laplacian defined as $L_{ij} = 1,\ i \neq j$, if node i and node j are connected, and $L_{ii} = \sum_j L_{ij}$. In [50], for each area α a reference node x_1^α is assigned and the fast variable z_α is defined as $z_\alpha[i-1] = x_1^\alpha - x_i^\alpha,\ i = 2, 3, \cdots, m_\alpha$, whereas the slow variable y is defined as in (5.24). With this change of variables a linear system in (y, z) coordinates is obtained, and is further exploited to reveal the time-scales. Unlike the analysis in [50] however, in our formulation we make explicit use of the graph incidence matrix D, and introduce an orthonormal transformation Q to define the fast variable z. With this approach we reveal a symmetric structure in (5.36)-(5.37) (due to $U^T D$ and $D^T U$ in (5.36), and QD and $D^T Q^T$ in (5.37)), which is the key to the nonlinear result proved in the next section.

5.5 Time-Scale Separation

In this section, we show that the smallness of the node and area parameters d and δ lead to a time-scale separation in (5.36)-(5.37). In particular, δ plays the role of a singular perturbation parameter and the node parameter d is a regular perturbation parameter which, when small, guarantees that the slow variables y are weakly coupled to the fast variables z, and that the contribution of the internal links to the aggregate model is small.

We reorder the incidence matrix D in such a way that the internal links constitute the first Γ^I columns of D, and the external links constitute the remaining Γ^E columns. More specifically, the first γ_1^I columns of D correspond to the internal links in area 1, columns $(\gamma_1^I + 1)$ to $(\gamma_1^I + \gamma_2^I)$ correspond to the internal links of area 2, etc. This ar-

rangement decomposes D into a block diagonal $N \times \Gamma^I$ matrix D^I with $m_\alpha \times \gamma_\alpha^I$ blocks of internal links, and an $N \times \Gamma^E$ matrix D^E of external links:

$$D = \left[\begin{array}{ccc|c} D_1^I & & & \\ & \ddots & & D^E \\ & & D_r^I & \end{array}\right] = \left[\begin{array}{c|c} D^I & D^E \end{array}\right]. \tag{5.39}$$

We further assume that in the area partitioning of Section 5.3 the graphs represented by D_α^I's and D^E are connected, i.e. the nodes in the same area, as well as the areas as aggregate nodes constitute connected graphs. Using the structure in (5.39), and noting that the sum of the rows of D is zero, we partition $U^T D$, Ψ and QD as:

$$U^T D = \left[\begin{array}{c|c} 0_{r\times\Gamma^I} & \Sigma \end{array}\right],\ \Psi = \left[\begin{array}{c} \Psi_I \\ \hline \Psi_E \end{array}\right],\ QD = \left[\begin{array}{c|c} A & B \end{array}\right], \tag{5.40}$$

where $\Sigma := U^T D^E$ is $r \times \Gamma^E$ corresponds to the external links, Ψ_I is $\Gamma^I \times 1$ and denotes the internal link nonlinearities, Ψ_E is $\Gamma^E \times 1$ and denotes the external link nonlinearities, $A := \mathrm{diag}(A_1,\ A_2,\ \ldots\ A_r)$ is $(N-r) \times \Gamma^I$, $A_\alpha = Q_\alpha D_\alpha^I$ is $(m_i - 1) \times \gamma_\alpha^E$ and corresponds to internal links of area α, and $B = QD^E$ is $(N-r) \times \Gamma^E$ and corresponds to the external links. With this partitioning, (5.36)-(5.37) becomes:

$$\dot{y} = -M_a^{-1}\Sigma\Psi_E(\Sigma^T y + B^T z) + M_a^{-1}U^T 1_N v(t) \tag{5.41}$$

$$\dot{z} = -A\Psi_I(A^T z) - B\Psi_E(\Sigma^T y + B^T z). \tag{5.42}$$

We now model the interarea dynamics as a dynamic network with the $r \times \Gamma^E$ matrix Σ in (5.41), that is, Σ is the incidence matrix of the graph that the areas, as aggregate nodes, constitute. Similar to Q_α's, we let R be an $(r-1) \times r$ matrix,

$$R := \Delta(r), \tag{5.43}$$

with orthonormal rows that are each orthogonal to 1_r; that is,

$$R1_r = 0, \quad RR^T = I_{r-1}. \tag{5.44}$$

We then define the area difference variable

$$\tilde{y} = Ry, \tag{5.45}$$

and note from (5.44) and (5.45) that

$$y \in \mathcal{R}(1_r) \Rightarrow \tilde{y} = 0, \tag{5.46}$$

which means that as the areas synchronize, the area difference variable $\tilde{y}$ converges to zero. Next, because $I_r - R^T R$ is an orthogonal projection matrix onto the span of 1_r, and because 1_r is in the null space of Σ^T, it follows that

$$\Sigma^T(I_r - R^T R) = 0 \Longrightarrow \Sigma^T = \Sigma^T R^T R \Longleftrightarrow \Sigma = R^T R \Sigma. \tag{5.47}$$

Using (5.41) and (5.47), and noting that

$$R M_a^{-1} U^T 1_N = 0, \tag{5.48}$$

we obtain

$$\dot{\tilde{y}} = -CR\Sigma\Psi_E(\Sigma^T R^T \tilde{y} + B^T z) =: F(\tilde{y}), \tag{5.49}$$

where

$$C := R M_a^{-1} R^T. \tag{5.50}$$

Therefore, in the $(\tilde{y}, z)$ coordinates, we have the dynamic system:

$$\begin{aligned} \dot{\tilde{y}} &= -CR\Sigma\Psi_E(\Sigma^T R^T \tilde{y} + B^T z) && (5.51) \\ \dot{z} &= -A\Psi_I(A^T z) - B\Psi_E(\Sigma^T R^T \tilde{y} + B^T z), && (5.52) \end{aligned}$$

where, as shown in Appendix B, the matrix norms satisfy

$$\begin{aligned} ||CR\Sigma||_\infty = ||RM_a^{-1}\Sigma||_\infty &\leq \frac{2\gamma^E}{m}, && (5.53) \\ ||A||_\infty = ||QD^I||_\infty &> c^I, && (5.54) \\ ||B||_\infty = ||QD^E||_\infty &\leq 2c^E. && (5.55) \end{aligned}$$

Table 5.1: Matrices characterizing z, y and $\tilde{y}$ dynamics

Matrix	Dimension	Comments
D	$N \times M$	Graph incidence matrix (nodes)
M_a	$r \times r$	$M_a = \text{diag}(m_1, m_2, \cdots, m_r)$
U	$N \times r$	$U = \text{diag}(1_{m_1}, 1_{m_2}, \cdots, 1_{m_r})$
Q_α	$(m_\alpha - 1) \times m_\alpha$	$Q_\alpha Q_\alpha^T = I_{m_\alpha - 1}$, $Q_\alpha 1_\alpha = 0$
Q	$(N - r) \times N$	$Q = \text{diag}(Q_1, Q_2, \cdots, Q_r)$
A	$(N - r) \times \Gamma^I$	$A = \text{diag}(Q_1 D_1^I, \cdots, Q_r D_r^I)$
B	$(N - r) \times \Gamma^E$	$B = QD^E$
Σ	$r \times \Gamma^E$	Graph incidence matrix (areas)
R	$(r - 1) \times r$	$RR^T = I_{r-1}$, $\Sigma^T R^T R = \Sigma^T$
Ψ_I	$\Gamma^I \times 1$	Ψ_I: Internal link nonlinearities
Ψ_E	$\Gamma^E \times 1$	Ψ_E: External link nonlinearities
C	$(r - 1) \times (r - 1)$	$C = RM_a^{-1}R^T$

To obtain an explicit singular perturbation model for (5.51)-(5.52), we define the fast and slow time-scales

$$t_f := c^I t \quad \text{and} \quad t_s := \delta t_f, \tag{5.56}$$

and rewrite (5.51)-(5.52) as

$$\frac{d\tilde{y}}{dt_s} = -\overline{C}R\Sigma\Psi_E(\Sigma^T R^T \tilde{y} + B^T z) =: F(\tilde{y}, z) \tag{5.57}$$

$$\delta\frac{dz}{dt_s} = -\overline{A}\Psi_I(A^T z) - d\overline{B}\Psi_E(\Sigma^T R^T \tilde{y} + B^T z) =: G(\tilde{y}, z, d) \tag{5.58}$$

where

$$\overline{A} := A/c^I, \quad \overline{B} := B/c^E, \quad \overline{C}R\Sigma =: CR\Sigma/(\delta c^I) \tag{5.59}$$

all have $\mathcal{O}(1)$ norms. We next identify the reduced and boundary-layer systems of the singular perturbation model in (5.57)-(5.58). Denoting the solution of the quasi-steady-state equation

$$0 = -\overline{A}\Psi_I(A^T z) - d\overline{B}\Psi_E(\Sigma^T R^T \tilde{y} + B^T z) =: f_d(\tilde{y}, z) \tag{5.60}$$

by

$$z = h(\tilde{y}), \tag{5.61}$$

we obtain the reduced model

$$\frac{d\tilde{y}}{dt_s} = -\overline{C}R\Sigma\psi_E(\Sigma^T R^T \tilde{y} + B^T h(\tilde{y})) = F(\tilde{y}, h(\tilde{y})). \tag{5.62}$$

The quasi steady state solution $z = h(\tilde{y})$ is indeed well-defined due to the monotonicity of $\Psi(\cdot)$ from (5.6), and the connectedness of the network, as will be explicitly shown in Step 1 of the proof of Theorem 1. Finally, with the variable

$$\xi := z - h(\tilde{y}), \tag{5.63}$$

the boundary-layer model is

$$\begin{aligned} \frac{d\xi}{dt_f} &= -\overline{A}\Psi_I(A^T\xi + A^T h(\tilde{y})) - d\overline{B}\Psi_E(B^T\xi + \Sigma^T R^T \tilde{y} + B^T h(\tilde{y})), \\ &= G(\tilde{y}, \xi + h(\tilde{y}), d) \end{aligned} \tag{5.64}$$

We now let $\tilde{y}_s(t_s)$ and $\xi_f(t_f)$ denote the solutions of the reduced and boundary-layer systems (5.62) and (5.64), respectively, and characterize how well $\tilde{y}_s(t_s)$ and $\xi_f(t_f)$ approximate the exact solution of the singularly perturbed system (5.57)-(5.58):

Theorem 5.1: *Consider the singular perturbation problem (5.57) - (5.58) and assume that ψ_k in (5.3) is twice continuously differentiable and uniformly monotone as in (5.6). Then, given compact sets $\Omega_{\tilde{y}} \subset \mathbb{R}^{r-1}$ and $\Omega_\xi \subset \mathbb{R}^{N-r}$, there exists a positive constant d^*, and for each $0 < d < d^*$ there exists a positive constant δ_d^* such that for all $t_0 \geq 0$, $\tilde{y}(t_0) \in \Omega_{\tilde{y}}$, $z(t_0) - h(\tilde{y}(t_0)) \in \Omega_\xi$, $0 < d < d^*$ and $0 < \delta < \delta_d^*$, the singular perturbation problem (5.57)-(5.58) has a unique solution $\tilde{y}(t_s)$, $z(t_s)$ on $[t_0,\ \infty)$, and*

$$\tilde{y}(t_s) - \tilde{y}_s(t_s) = \mathcal{O}(\delta) \tag{5.65}$$

$$z(t_s) - h(\tilde{y}_s(t_s)) - \xi_f(t_f) = \mathcal{O}(\delta) \tag{5.66}$$

hold uniformly for $t \in [t_0,\ \infty)$. Moreover, given any $t_b > t_0$, there exist $\delta_d^{**} < \delta_d^*$ such that

$$z(t_s) - h(\tilde{y}_s(t_s)) = O(\delta) \tag{5.67}$$

hold uniformly for $t \in [t_b,\ \infty)$ whenever $\delta < \delta_d^{**}$. □

Theorem 1 implies that for sufficiently small network parameters d and δ, the nodes within the same area synchronize in the fast time-scale, and the areas behave as aggregate

nodes in the slow time scale. We wish to emphasize that once a network and area partitions are given, d and δ are fixed parameters and cannot be adjusted. Therefore, Theorem 1 should be interpreted as a conceptual result that justifies a reduced model based on aggregate areas when d and δ are indeed small.

Proof of Theorem 5.1: To prove Theorem 1, we will follow [51, Thm. 11.2], and show that each assumption therein is satisfied by the singularly perturbed system (5.57)-(5.58). In particular, Step 1 proves the existence and uniqueness of the solution $z = h(\tilde{y})$ for the quasi-steady-state equation (5.60). In Steps 2 and 3, we show that given $\Omega_{\tilde{y}}$ and Ω_ξ, we can find compact sets $S_{\tilde{y}} \supset \Omega_{\tilde{y}}$ and $S_\xi \supset \Omega_\xi$, and a positive number d^* such that, whenever $d < d^*$, the reduced and the boundary-layer systems are exponentially stable with regions of attraction including $S_{\tilde{y}}$ and S_ξ. We note that the regularity assumptions in [51, Thm. 11.2] are satisfied by (5.57)-(5.58) since Ψ is twice continuously differentiable.

Step 1. Isolated solution for the quasi-steady-state equation: We recall from (5.60) that the quasi-steady-state equation for z is

$$0 = f_d(\tilde{y}, z) = \overline{A}\Psi_I(A^T z) + d\overline{B}\Psi_E(\Sigma^T R^T \tilde{y} + B^T z) \tag{5.68}$$

where both $\overline{A}$ and $\overline{B}$ are $\mathcal{O}(1)$. We now show that (5.68) has a unique solution of the form $z = h(\tilde{y})$.

To prove the existence of a solution of the form $z = h(\tilde{y})$ that satisfies $f_d(\tilde{y}, h(\tilde{y})) = 0$, we exploit a uniform monotonicity [103] property of $f_d(\tilde{y}, z)$. To this end, we recall that ψ_k' is uniformly monotone by assumption (5.6), which implies the uniform monotonicity of Ψ_E' and Ψ_I'; that is,

$$\psi_k' \geq \epsilon \quad \Rightarrow \quad \Psi' = \left[\begin{array}{c} \Psi_I' \\ \hline \Psi_E' \end{array}\right] \geq \epsilon I_M \Rightarrow \Psi_I' \geq \epsilon I_{\Gamma^I} \text{ and } \Psi_E' \geq \epsilon I_{\Gamma^E} \tag{5.69}$$

To prove uniform monotonicity of $f_d(\tilde{y}, z)$ we pick an arbitrary vector $v \neq 0$ and obtain, using (5.69),

$$\begin{aligned} v^T \frac{\partial f_d}{\partial z} v &= v^T(\overline{A}\Psi_I' A^T + d\overline{B}\Psi_E' B^T)v \\ &\geq \epsilon \left(\lambda_{\min}(\overline{A}A^T) + d\lambda_{\min}(\overline{B}B^T)\right) v^T v. \end{aligned} \tag{5.70}$$

We also note from [83, Item 4e and Cor. 6.5] and [17] that $\lambda_{\min}(\overline{A}A^T) > 0$ since D_α^I's in (5.39) represent a connected graph by assumption. Therefore, there exists a $\bar{d}$ such that

for all $d < \bar{d}$, the $\tilde{y}$-independent modulus in (5.70) is positive, that is

$$d < \bar{d} \Longrightarrow \epsilon \left(\lambda_{\min}(\overline{A} A^T) + d\lambda_{\min}(\overline{B} B^T) \right) > 0, \tag{5.71}$$

which proves the uniform monotonicity of $f_d(\tilde{y}, z)$ in z. We then conclude from [103, Thm. 5.4.5] that f_d is a homeomorphism, and that there exists a unique $z = h(\tilde{y})$ such that $f_d(\tilde{y}, z) = 0$. Moreover, since $\frac{\partial f_d}{\partial \tilde{y}}$ exists, $h(\tilde{y})$ is a differentiable function of $\tilde{y}$. Specifically,

$$\frac{\partial f_d}{\partial z}\frac{\partial z}{\partial \tilde{y}} + \frac{\partial f_d}{\partial \tilde{y}} = 0 \Rightarrow \ \frac{\partial h(\tilde{y})}{\partial \tilde{y}} = -\left(\frac{\partial f_d}{\partial z}\right)^{-1} \frac{\partial f_d}{\partial \tilde{y}}, \tag{5.72}$$

where $z = h(\tilde{y})$, and $\left(\frac{\partial f_d}{\partial z}\right)^{-1}$ is well defined due to (5.70) and (5.71).

Step 2. Exponential stability of the reduced system: To prove exponential stability of the reduced model in (5.62) we take the Lyapunov function

$$V(\tilde{y}) = \frac{1}{2}\tilde{y}^T P \tilde{y}, \tag{5.73}$$

where

$$P = P^T := \overline{C}^{-1} = \delta c^I (R M_a^{-1} R^T)^{-1} > 0, \tag{5.74}$$

and let $S_{\tilde{y}}$ denote a level set of $V(\tilde{y})$ such that $\Omega_{\tilde{y}} \subset S_{\tilde{y}}$. We note from the Mean Value Theorem that $F(\tilde{y})$ in (5.62) can be represented as :

$$F(\tilde{y}) = \int_0^1 \frac{\partial F}{\partial \tilde{y}}(\lambda \tilde{y}) \tilde{y} d\lambda. \tag{5.75}$$

Then, the time derivative of V becomes:

$$\begin{aligned} \frac{dV}{dt_s} &= \frac{1}{2}\tilde{y}^T P \int_0^1 \frac{\partial F}{\partial \tilde{y}}(\lambda \tilde{y}) \tilde{y} d\lambda + \frac{1}{2}\left(\int_0^1 \frac{\partial F}{\partial \tilde{y}}(\lambda \tilde{y}) \tilde{y} d\lambda \right)^T P \tilde{y} \\ &= \frac{1}{2}\tilde{y}^T \left(\int_0^1 \left(P \frac{\partial F}{\partial \tilde{y}}(\lambda \tilde{y}) + \frac{\partial F}{\partial \tilde{y}}^T (\lambda \tilde{y}) P \right) d\lambda \right) \tilde{y}. \end{aligned} \tag{5.76}$$

We note that dV/dt_s is negative definite if $P\partial F/\partial \tilde{y} + (\partial F/\partial \tilde{y})^T P < 0$ uniformly in λ.

Using (5.72), we obtain

$$\begin{aligned} P\frac{\partial F}{\partial \tilde{y}} &= -\overline{C}^{-1}\left(\overline{C}R\Sigma\Psi'_E\Sigma^T R^T - \overline{C}R\Sigma\Psi'_E B^T\frac{\partial h(\tilde{y})}{\partial \tilde{y}}\right) \\ &= -R\Sigma\left\{\Psi'_E - d\Psi'_E B^T\left(\overline{A}\Psi'_I A^T + d\overline{B}\Psi'_E B^T\right)^{-1}\overline{B}\Psi'_E\right\}\Sigma^T R^T. \end{aligned} \tag{5.77}$$

From the symmetry in (5.77) we conclude that $P\partial F/\partial\tilde{y} + (\partial F/\partial\tilde{y})^T P = 2P\partial F/\partial\tilde{y}$. Since $S_{\tilde{y}}$ is compact, we can find an upper bound on Ψ'_E for $\tilde{y} \in S_{\tilde{y}}$. Moreover, a lower bound on Ψ'_I and Ψ'_E already exists from (5.69); therefore, we can find a $d^* \leq \bar{d}$ such that for all $d < d^*$,

$$\Psi'_E > d\Psi'_E B^T\left(\overline{A}\Psi'_I A^T + d\overline{B}\Psi'_E B^T\right)^{-1}\overline{B}\Psi'_E, \tag{5.78}$$

and consequently,

$$\dot{V} < -\sigma_r \tilde{y}^T\tilde{y}, \tag{5.79}$$

for some $\sigma_r > 0$. Therefore, we conclude that for all $d < d^*$, $S_{\tilde{y}}$ is invariant and the reduced model is exponentially stable in $S_{\tilde{y}}$.

Step 3. Exponential stability of the boundary-layer system: To prove exponential stability of the boundary-layer model in (5.64) we take the Lyapunov function

$$V_b(\xi) = \frac{1}{2}\xi^T\xi, \tag{5.80}$$

and let S_ξ denote a level set of $V(\xi)$ such that $\Omega_\xi \subset S_\xi$. We then obtain

$$\frac{dV_b}{dt_f} = -\xi^T\left(\int_0^1 (\overline{A}\Psi'_I A^T + d\overline{B}\Psi'_E B^T)d\lambda\right)\xi \tag{5.81}$$

where we use the fact that

$$G(\tilde{y},\xi) = \int_0^1 \frac{\partial G}{\partial \xi}(\tilde{y},\lambda\xi)\xi d\lambda \tag{5.82}$$

and

$$\frac{\partial G}{\partial \xi} = \frac{\partial G}{\partial \xi}^T = -\overline{A}\Psi'_I A^T - d\overline{B}\Psi'_E B^T. \tag{5.83}$$

Using (5.69) and (5.71), we conclude that for all $d < d^* \leq \bar{d}$ and $\xi \in S_\xi$

$$\frac{dV_b}{dt_f} \leq -\sigma_b \xi^T \xi, \tag{5.84}$$

for some $\sigma_b > 0$, therefore, S_ξ is invariant and $\xi = 0$ is exponentially stable in S_ξ.

Through Steps 1 to 3, we proved that the assumptions in [51, Thm. 11.2] are satisfied by (5.57)-(5.58) and (5.62)-(5.64), thus, the approximation results (5.65)-(5.66) and (5.67) follows from [51, Thm. 11.2]. □

5.6 Summary

We studied a nonlinear agreement problem and revealed the time-scale properties induced by the sparse and dense link structure of the network. We showed that for sufficiently small d and δ, densely linked nodes within the same area synchronize in the fast-time scale, and the reduced model obtained by aggregate nodes represents the long-term behavior of the overall network. We envision applications of this result in obtaining computationally tractable models to analyze and simulate molecular dynamics, large swarms of robotic vehicles, animal aggregations, and data fusion in sensor networks.

CHAPTER 6
CONCLUSIONS AND FUTURE RESEARCH DIRECTIONS

In this thesis, we have pursued analysis and design tools for coordination of nonlinear multi-agent systems. We first reviewed a unifying passivity framework for the group agreement problem and extended it to a class of sampled-data systems in Chapter 3. The sampled-data result is of particular importance because, in practice, the communication channel between the members of the group may necessitate a discrete-time implementation in the feedforward path, whereas in the feedback path the local controllers or internal dynamics of each member may be continuous-time. We showed that in such sampled-data implementations the size of the region of attraction is determined by the sampling period and the feedback gain. We plan to extend our design to other classes of sampled-data systems. Robustness against time-delay that occur in the communication links is an important problem that will be addressed in future work. An important flexibility in the feedback law (2.3) is the filter $\mathcal{H}_i$ which can be exploited to achieve enhanced robustness and performance properties.

In Chapter 4, we considered a combined gradient climbing and formation design, and showed that if there is sufficient time-scale separation between the slow gradient motion and the fast dither motion, the formation dynamics act as a boundary layer system relative to the leader vehicle dynamics. The leaders velocity is introduced in a parameterized form so that an adaptive reconstruction can be pursued by the rest of the vehicles to follow the gradient motion while averaging out dither motion. Currently, gradient climbing methods for formations of underactuated vehicles, and robust redesigns that address the effect of the external disturbances such as wind and flow are being developed. We will further study dynamic field distributions for tracking a slowly varying/moving maxima which is an important problem in practice.

We finally studied a nonlinear agreement problem in Chapter 5 and revealed the time-scale properties induced by the sparse and dense link structure of the network. We showed that for sufficiently small d and δ, densely linked nodes within the same area synchronize in the fast-time scale, and the reduced model obtained by aggregate nodes represents the long-term behavior of the overall network. This result can be applied in obtaining computationally tractable models to analyze and simulate molecular dynamics, large swarms of robotic vehicles, animal aggregations, and data fusion in sensor networks.

We are currently extending our time-scale separation results to networks with directed links, and this dense/sparse decomposition method is particularly promising for order reduction of Markov chains. Among numerous applications that would benefit from this novel Markov chain reduction technique are stochastic models of biochemical reaction networks [104], which are preferable to deterministic models at low molecular concentrations.

REFERENCES

[1] N.E. Leonard and E. Fiorelli. Virtual leaders, artificial potentials and coordinated control of groups. In *Proceedings of the 40th IEEE Conference on Decision and Control*, pages 2968–2973, Orlando, Florida, 2001.

[2] P. Ögren, E. Fiorelli, and N.E. Leonard. Cooperative control of mobile sensor networks: Adaptive gradient climbing in a distributed network. *IEEE Transactions on Automatic Control*, 49(8):1292–1302, 2004.

[3] V. Gazi and K.M. Passino. Stability analysis of social foraging swarms. *IEEE Transactions on Systems, Man, and Cybernetics*, 34(1):539–557, 2004.

[4] A. Jadbabaie, J. Lin, and A.S. Morse. Coordination of groups of mobile autonomous agents using nearest neighbor rules. *IEEE Transactions on Automatic Control*, 48(6):988–1001, 2003.

[5] R. Olfati-Saber and R.M. Murray. Consensus protocols for networks of dynamic agents. In *Proceedings of the American Control Conference*, pages 951–956, Denver, Colorado, 2003.

[6] R. Olfati-Saber and R.M. Murray. Consensus problems in networks of agents with switching topology and time-delays. *IEEE Transactions on Automatic Control*, 49(9):1520–1533, 2004.

[7] L. Moreau. Stability of multiagent systems with time-dependent communication links. *IEEE Transactions on Automatic Control*, 50(2):169–182, 2005.

[8] S. Roy, A. Saberi, and K. Herlugson. A control-theoretic perspective on the design of distributed agreement protocols. In *Proceedings of the American Control Conference*, pages 1672–1679, Portland, OR, 2005.

[9] L. Xiao and S. Boyd. Fast linear iterations for distributed averaging. *Systems and Control Letters*, 53:65–78, 2004.

[10] R. Olfati-Saber. Flocking for multi-agent dynamic systems: Algorithms and theory. *IEEE Transactions on Automatic Control*, 51(3):401–420, 2006.

[11] C.W. Reynolds. Flocks, herds, and schools: A distributed behavioral model. *Computer Graphics*, 21:25–34, 1987.

[12] D.W. Casbeer, D.B. Kingston, R.W. Beard, S.-M. Li T.W. McLain, and R. Mehra. Cooperative forest fire surveillance using a team of small unmanned air vehicles. *International Journal of Systems Sciences*, 37(6):351–360, 2006.

[13] J.A. Fax and R.M. Murray. Information flow and cooperative control of vehicle formations. *IEEE Transactions on Automatic Control*, 49(9):1465–1476, 2004.

[14] H.G. Tanner, G.J. Pappas, and V. Kumar. Leader-to-formation stability. *IEEE Transactions on Robotics and Automation*, 20(3):443–455, 2004.

[15] J.A. Marshall, M.E. Broucke, and B.A. Francis. Formation of vehicles in cyclic pursuit. *IEEE Transactions on Automatic Control*, 49(11):1963–1974, 2004.

[16] D. B. Kingston and R.W. Beard. Discrete-time average-consensus under switching network topologies. In *Proceedings of the American Control Conference*, pages 3551–3556, Minneapolis, MN, 2006.

[17] M. Arcak. Passivity as a design tool for group coordination. *IEEE Transactions on Automatic Control*, 52(8):1380–1390, 2007.

[18] Z. Lin, B. Francis, , and M. Maggiore. State agreement for coupled nonlinear systems with time-varying interaction. 2006.

[19] D. Angeli and P.-A Bliman. Extension of a result by moreau on stability of leaderless multi-agent systems. In *Proceedings of the 44th IEEE Conference on Decision and Control*, pages 759–764, Seville, Spain, 2005.

[20] J.H. Chow (ed). *Time Scale Modelling of Dynamic Networks with Applications to Power Systems*. Lecture Notes in Control and Information Sciences, vol.46. Springer–Verlag, New York, 1982.

[21] P. V. Kokotović. Subsystems, time-scales and multimodeling. *Automatica*, 17(6):789–795, 1981.

[22] P. V. Kokotović, B. Abramovic, J.H. Chow, and J.R. Winkelman. Coherency based decomposition and aggregation. *Automatica*, 18(1):47–56, 1982.

[23] R. H. Phillips and P. V. Kokotović. A singular perturbation approach to modeling and control of markov chains. *IEEE Transactions on Automatic Control*, 26(5):1087–1094, 1981.

[24] F. Delebecque, J. P. Quadrat, and P. V. Kokotović. A unified view of aggregation and coherency in networks and markov chains. *International Journal of Control*, 40(5):939–952, 1984.

[25] G. G. Yin and Q. Zhang. *Continuous-time Markov Chains and Applications: A Singular Perturbation Approach*. Springer, New York, 1998.

[26] U. Alon. *An introduction to systems biology: Design principles of biological circuits*. Chapman Hall, New York, 2006.

[27] A.W. Rives and T. Galitski. Modular organization of cellular networks. *Proceedings of National Academy of Science*, 100(3):1128–1133, 2003.

[28] H.H. McAdams and L. Shapiro. A bacterial cell-cycle regulatory network operating in time and space. *Science*, 301(5641):1874–1877, 2003.

[29] D. Thieffry and D. Romero. The modularity of biological regulatory networks. *BioSystems*, 50:49–59, 1999.

[30] E. Ravazs, A.L. Somera, D.A. Mongru, Z.N. Oltvai, and A.-L. Barábasi. Hierarchical organization of modularity in metabolic networks. *Science*, 297(5586):1551–1555, 2002.

[31] S.W. Pacala, D.M. Gordon, and H.C.J. Godfray. Effects of social group size on information transfer and task allocation. *Evolutional Ecology*, 10:127–165, 1996.

[32] E. Bonabeau, G. Theraulaz, and J.-L. Deneubourg. Group and mass recruitment in ant colonies: the influence of contact rates. *Journal of Theoretical Biology*, 195(2):157–166, 1998.

[33] F. Zhao and L. Guibas. *Wireless Sensor Networks: An Information Processing Approach*. Morgan Kaufmann, San Francisco, CA, 2004.

[34] D.S. Laila, D. Nešić, and A.R. Teel. Open and closed loop dissipation inequalities under sampling and controller emulation. *European Journal of Control*, 8(2):109–125, 2002.

[35] I-A.F. Ihle, M. Arcak, and T.I. Fossen. Passivity-based designs for synchronized path following. *Automatica*, 43(9):1508–1518, 2007.

[36] R. Bachmayer and N.E. Leonard. Vehicle networks for gradient descent in a sampled environment. In *Proceedings of the 41st IEEE Conference on Decision and Control*, pages 113–117, Las Vegas, NV, 2002.

[37] J. Cortés, S. Martínez, T. Karataş, and F. Bullo. Coverage control for mobile sensing networks. *IEEE Transactions on Robotics and Automation*, 20(2):243–255, 2004.

[38] D.F. Chichka, J. Speyer, and C.G. Park. Peak seeking control with application to formation flight. In *Proceedings of the 38th IEEE Conference on Decision and Control*, Phoenix, AZ, 1999.

[39] P. Binetti, K. B. Ariyur, M. Krstić, and F. Bernelli. Control of formation flight via extremum seeking. In *Proceedings of the 2002 American Control Conference*, Anchorage, AK, 2002.

[40] K.B. Ariyur and M. Krstić. *Real-Time Optimization by Extremum-Seeking Feedback*. Wiley-Interscience, Hoboken, NJ, 2003.

[41] A.R. Teel and D. Popović. Solving smooth and nonsmooth multivariable extremum seeking problems by the methods of nonlinear programming. In *Proceedings of the 2001 American Control Conference*, pages 2394–2399, Arlington, VA, 2001.

[42] Y. Tan, D. Nešić, and I. Mareels. On non-local stability properties of extremum seeking control. *Automatica*, 42(6):889–903, 2006.

[43] K.M. Passino. Biomimicry of bacterial foraging for distributed optimization and control. *IEEE Control Systems Magazine*, 22(3):52–67, 2002.

[44] L. R. Shugart, J. F. McCarthy, and R. S. Halbrook. Biological markers of environmental and ecological contamination: An overview. *Risk Analysis*, 12(3):353–360, 1992.

[45] C. Zhang, A. Siranosian, and M. Krstić. Extremum seeking for moderately unstable systems and for autonomous target tracking without position measurements. In *Proceedings of the American Control Conference*, Minneapolis, MN, 2006.

[46] C. Zhang, D. Arnold, N. Ghods, A. Siranosian, and M. Krstić. Source seeking with nonholonomic unicycle without position measurement–part I: Tuning of forward velocity. In *Proceedings of the 45th IEEE Conference on Decision and Control*, pages 3040–3045, San Diego, CA, 2006.

[47] T. Huntsberger, P. Pirjanian, A. Trebi-Ollennu, H. D. Nayar, H. Aghazarian, A. J. Ganino, M. Garrett, S. S. Joshi, and P. S. Schenker. Campout: A control architecture for tightly coupled coordination of multirobot systems for planetary surface exploration. *IEEE Transactions on Systems, Man, and Cybernetics-Part A: Systems and Humans*, 33(5):550–559, 2003.

[48] A.R. Teel, L. Moreau, and D. Nešić. A unified framework for input-to-state stability in systems with two time scales. *IEEE Transactions on Automatic Control*, 48:1526–1544, 2003.

[49] H.A. Simon and A. Ando. Aggregation of variables in dynamic systems. *Econometrica*, 29:111–138, 1961.

[50] J. H. Chow and P. V. Kokotović. Time scale modeling of sparse dynamic networks. *IEEE Transactions on Automatic Control*, 30(8):714–722, 1985.

[51] H. K. Khalil. *Nonlinear Systems*. Prentice Hall, Upper Saddle River, NJ, third edition, 1997.

[52] O. Brune. Synthesis of a finite two-terminal network whose driving-point impedance is a prescribed function of frequency. *Journal of Mathematics and Physics*, 10:191–236, 1931.

[53] R. E. Kalman. Lyapunov functions for the problem of Lur'e in automatic control. *Proceedings of the National my of Science*, 49:201–205, 1963.

[54] V. A. Yakubovich. The frequency theorem in control theory. *Siberian Mathematical Journal*, 14:384–419, 1973.

[55] V.M. Popov. Absolute stability of nonlinear systems of automatic control. *Automation and Remote Control*, 22:857–875, 1962. Translated from *Avtomatika i Telemekhanika*, 22:961–979, 1961.

[56] J.C. Willems. Dissipative dynamical systems, Part i: General theory; Part ii: Linear systems with quadratic supply rates. *Archive for Rational Mechanics and Analysis*, 45:321–393, 1972.

[57] M. Janković, M. Larsen, and P.V. Kokotović. Master-slave passivity design for stabilization of nonlinear systems. In *Proceedings of the 18th American Control Conference*, pages 769–773, San Diego, CA, 1999.

[58] G. Zames. On the input-output stability of time-varying nonlinear feedback systems-Parts I and II. *IEEE Transactions on Automatic Control*, 11:228–238 and 465–479, 1966.

[59] F.H. Clarke, Y.S. Ledyaev, E.D. Sontag, and A.I. Subbotin. Asymptotic controllability implies feedback stabilization. *IEEE Transactions on Automatic Control*, 42(10):1394–1407, 1997.

[60] B.Castillo, S. Di Gennaro, S.Monaco, and D. Normand-Cyrot. On regulation under sampling. *IEEE Transactions on Automatic Control*, 42(6):864–868, 1997.

[61] A.M. Dabroom and H.K. Khalil. Output feedback sampled-data control of nonlinear systems using high-gain observers. *IEEE Transactions on Automatic Control*, 46(11):1712–1725, 1997.

[62] I.M.Y. Mareels, H.B. Penfold, and R.J. Evans. Controlling nonlinear time-varying systems via Euler approximations. *Automatica*, 28(4):681–696, 1992.

[63] D. Nešić, A.R. Teel, and P.V.Kokotović. Sufficient conditions for stabilization of sampled-data nonlinear systems via discrete-time approximations. *Systems and Control Letters*, 38(5):259–270, 1999.

[64] D. Nešić and A.R. Teel. A framework for stabilization of nonlinear sampled-data systems based on their approximate discrete-time models. *IEEE Transactions on Automatic Control*, 49(7):1103–1041, 2004.

[65] I.G. Polushin and H.J. Marquez. Multirate versions of sampled-data stabilization of nonlinear systems. *Automatica*, 40(6):1035–1041, 2001.

[66] P. Astuti, M. Corless, and D. Williamson. On the convergence of sampled data nonlinear systems. *Differential Equations: Theory, Numerics and Applications*, Eds. E. Van Groesen and E. Soewono, pages 201–210. Kluwer, The Netherlands, 2004.

[67] D.H. Owen, Y. Zheng, and S.A. Billings. Fast sampling and stability of nonlinear sampled-data systems: Part 1. existence theorems. *IMA Journal of Mathematical Control and Information*, 7:1–11, 1990.

[68] Y. Zheng, D.H. Owen, and S.A. Billings. Fast sampling and stability of nonlinear sampled-data systems: Part 2. sampling rate estimation. *IMA Journal of Mathematical Control and Information*, 7, 1990.

[69] D. Nešić, A.R. Teel, and E.D. Sontag. Formulas relating $\mathcal{KL}$-stability estimates of discrete-time and sampled-data nonlinear systems. *Systems and Control Letters*, 38(1):49–60, 1999.

[70] N.N. Bogoliuboff and Y.A. Mitropolskii. *Asymptotic methods in the theroy of nnlinear oscillators*. Gordon Breach, New York, 1961.

[71] P.R. Sethna. Method of averaging for systems bounded for positive time. *Journal of Mathematical Analysis and Applications*, 41:621–631, 1973.

[72] J.K. Hale. *Ordinary differential equations*. Krieger, Huntington, New York, 1980.

[73] V.I. Arnold. *Geometrical Methods in the Theory of Ordinary Differantial Equations*. Springer Verlag, Berlin, 1983.

[74] J.K. Guckenheimer and P.J. Holmes. *Nonlinear Oscillations, Dynamical Systems and Bifurcations of Vector Fields*. Springer Verlag, Berlin, 1983.

[75] C. Zhang, A. Siranosian, and M. Krstić. Extremum seeking for moderately unstable systems and for autonomous target tracking without position measurements. In *Proceedings of the American Control Conference*, Minneapolis, MN, 2006.

[76] M.I. Freedman and J.L. Kaplan. Singular perturbations of two point boundary value problems arising in optimal control. *SIAM Journal on Control and Optimization*, 14:189, 1976.

[77] K.V. Kirkorian and C.T. Leondes. Application singular perturbations to optimal control. *Control and Dynamic Systems*, 18:131, 1982.

[78] A. Bensoussan. Singular perturbation results for a class of stochastic control problems. *IEEE Transactions on Automatic Control*, 26:1071, 1981.

[79] M. El-Ansary and H.K. Khalil. Reduced order modeling of nonlinear singularly perturbed systems driven by wide-band noise. In *Proceedings of the 21st IEEE Conference on Decision and Control*, pages 1090–1094, Orlando, FL, 1982.

[80] H.K. Khalil and A. Saberi. Decentralized stabilization of nonlinear interconnected systems using high gain feedback. *IEEE Transactions on Automatic Control*, 27:265, 1982.

[81] H.K. Khalil and F. Esfandiari. Semiglobal stabilization of a class of nonlinear systems using output feedback. *IEEE Transactions on Automatic Control*, 38:1412–1415, 1993.

[82] F. Delebecque, J. P. Quadrat, and P. V. Kokotović. Aggregability of synamic systems and lumpability of Markov chains. In *Proceedings of the 20st IEEE Conference on Decision and Control*, pages 199–203, San Diego, CA, 1981.

[83] N. Biggs. *Algebraic Graph Theory*. Cambridge University Press, second edition, 1993.

[84] A. J. van der Schaft. *L_2-gain and Passivity Techniques in Nonlinear Control*. Springer-Verlag, New York and Berlin, second edition, 2000.

[85] M. Janković R. Sepulchre and P. Kokotović. *Constructive Nonlinear Control*. Springer-Verlag, New York, 1997.

[86] A. P. Aguiar, J. P. Hespanha, and P. V. Kokotović. Path-following for non-minimum phase systems removes performance limitations. *IEEE Transactions on Automatic Control*, 50(2):234–239, 2005.

[87] K. D Do, J. P. Zhang, and J. Pan. Robust adaptive path-following of underactuated ships. In *Proceedings of the 41st IEEE Conference on Decision and Control*, pages 3243–3248, Las Vegas, NV, 2002.

[88] J. Hauser and R. Hindman. Maneuver regulation from trajectory tracking: Feedback linearizable systems. In *Proceedings of the IFAC Symposium on Nonlinear Control Systems Design*, pages 595–600, Lake Tahoe, CA, USA, 1995.

[89] C. Samson. Path following and time-varying feedback stabilization of a wheeled mobile robot. In *Proceedings of the ICARCV'92*, Singapore, 1992.

[90] R. Skjetne, T. I. Fossen, and P. V. Kokotović. Robust output maneuvering for a class of nonlinear systems. *Automatica*, 40(3):373–383, 2004.

[91] T. I. Fossen. *Marine control systems: Guidance, navigation and control of ships, rigs and underwater vehicles.* Marine Cybernetics, Trondheim, Norway, 2002.

[92] J. Nocedal and S.J. Wright. *Numerical Optimization.* Springer-Verlag, New York, 1999.

[93] J.C. Spall. Multivariable stochastic approximation using a simultaneous perturbation gradient approximation. *IEEE Transactions on Automatic Control*, 37(3):332–341, 1992.

[94] J.C. Spall. Adaptive stochastic approximation by the simultaneous perturbation method. *IEEE Transactions on Automatic Control*, 45(10):1839–1853, 2000.

[95] H. Bai., M. Arcak, and J.T. Wen. Group coordination when the reference velocity is available only to the leader: an adaptive design. In *Proceedings of the 2007 American Control Conference*, pages 5400–5405, New York, NY, 2007.

[96] C. Zhang and R. Ordóñez. Numerical optimization-based extremum seeking control of LTI systems. In *Proceedings of the 44th IEEE Conference on Decision and Control*, Sevilla, Spain, MN, 2006.

[97] C. Zhang and R. Ordóñez. Extremum seeking control based on numerical optimization and state regulation–part I: Theory and framework. In *Proceedings of the 45th IEEE Conference on Decision and Control*, pages 4466–4471, San Diego, CA, 2006.

[98] J.E. Dennis and R.B. Schnabel. *Numerical Methods for Unconstrained Optimization and Nonlinear Equations.* SIAM, Philadelphia, 1996.

[99] J. Kiefer and J. Wolfowitz. Stochastic estimation of a regression function. *Annals of Mathematical Statistics*, 23:462–466, 1952.

[100] J.R. Blum. Multidimensional stochastic approximation methods. *Annals of Mathematical Statistics*, 25:737–744, 1954.

[101] J. H. Chow, J. Cullum, and R. A. Willoughby. A sparsity based technique for identifying slow-coherent areas in large power systems. *IEEE Transactions on Power Apparatus and Systems*, 103(3):463–473, 1984.

[102] R. A. Date and J. H. Chow. Aggregation properties of linearized two-time-scale power networks. *IEEE Transactions on Circuits and Systems*, 38(7):720–730, 1991.

[103] J. M. Ortega and W. C. Rheinboldt. *Iterative Solution of Nonlinear Equations in Several Variables*. SIAM, Philadelphia, 2000.

[104] D.T. Gillespie. A rigorous derivation of the chemical master equation. *Physica A*, 188:404–425, 1992.

[105] C.T. Kelley. *Iterative Methods for Linear and Nonlinear Equations*. SIAM, Philadelphia, 1995.

APPENDIX A
PROOF OF LEMMA 4.1

To prove Lemma 4.1 we use the standard tools from multivariable calculus and unconstrained optimization theory. We let γ_1 and γ_2 denote the Lipschitz constants of $\nabla F(x)$ and $\nabla^2 F(x)$, respectively, for $x \in \mathcal{D} \subseteq \mathbb{R}^n$. Then, the finite difference approximations in (4.1) and (4.2) satisfy [98, Ch.5]

$$||G_k - \nabla F(x_k)||_1 \leq \frac{1}{2}\gamma_1 h_k \tag{A.1}$$

$$||H_k - \nabla^2 F(x_k)||_1 \leq \frac{5}{3} n \gamma_2 h_k. \tag{A.2}$$

We prove by induction. For $k = 0$, we first show that H_0 is nonsingular. We let $\epsilon \leq r$, $h_k \leq \bar{h}$ and

$$\epsilon + \frac{5}{3} n \bar{h} \leq \frac{\nu}{\beta \gamma_2}, \quad \nu < 1, \tag{A.3}$$

where $\nu < 1$ is to be selected. To show that H_0 is nonsingular, we employ the Banach Lemma given in [105, Theorem 1.2.1]. We first show that, with ϵ and $\bar{h}$ satisfying (A.3), $||\nabla^2 F(x^*)^{-1} H_0 - I|| < 1$ as follows:

$$\begin{aligned} ||\nabla^2 F(x^*)^{-1} H_0 - I|| &= ||\nabla^2 F(x^*)^{-1}(H_0 - \nabla^2 F(x^*))|| \\ &\leq ||\nabla^2 F(x^*)^{-1}|| \left[||H_0 - \nabla^2 F(x_0)|| \right. \\ &\quad \left. + ||\nabla^2 F(x_0) - \nabla^2 F(x^*)|| \right] \\ &\leq \beta \left(\frac{5}{3} n \gamma_2 \bar{h} + \gamma_2 \epsilon \right) \\ &\leq \beta \gamma_2 \left(\epsilon + \frac{5}{3} n \bar{h} \right) \leq \nu < 1. \end{aligned} \tag{A.4}$$

Hence, Banach Lemma implies

$$H_0^{-1} \leq \frac{||\nabla^2 F(x^*)^{-1}||}{1 - ||\nabla^2 F(x^*)^{-1} H_0 - I||} \leq \frac{\beta}{1 - \nu}. \tag{A.5}$$

Therefore, H_0 is nonsingular and x_1 is well defined. Next, we derive a bound on $||x_1 - x^*||$:

$$\begin{aligned}
||x_1 - x^*|| &= ||x_0 + H_0^{-1}G_0 - x^*|| \\
&\leq ||H_0^{-1}|| \Big\{ ||H_0(x_0 - x^*) - \nabla^2 F(x_0)(x_0 - x^*)|| \\
&\quad + ||\nabla F(x_0) - \nabla F(x^*) + \nabla^2 F(x_0)(x_0 - x^*)|| \\
&\quad + ||G_0 - \nabla F(x_0)|| \Big\} \\
&\leq \frac{\beta}{1-\nu} \left(\tfrac{5}{3} n \gamma_2 \bar{h} ||x_0 - x^*|| + \tfrac{\gamma_2}{2} ||x_0 - x^*||^2 + \tfrac{\gamma_1 \bar{h}}{2} \right) \\
&\leq \frac{\beta \gamma_2}{1-\nu} \left(\frac{5}{3} n \bar{h} + \frac{\epsilon}{2} \right) ||x_0 - x^*|| + \frac{\beta \gamma_1 \bar{h}}{2(1-\nu)} \\
&\leq \frac{\nu}{1-\nu} ||x_0 - x^*|| + \frac{\beta \gamma_1 \bar{h}}{2(1-\nu)}, \qquad \text{(A.6)}
\end{aligned}$$

which further restricts ν to be $\nu < \frac{1}{2}$ for convergence. Note that, we want $||x_1 - x^*|| \leq \epsilon$ as well, hence ν, $\bar{h}$ and ϵ must satisfy:

$$\frac{\nu}{1-\nu}\epsilon + \frac{\beta \gamma_1 \bar{h}}{2(1-\nu)} \leq \epsilon \Longrightarrow \epsilon(1 - 2\nu) \geq \beta \gamma_1 \bar{h}. \qquad \text{(A.7)}$$

We thus pick $\bar{h}$ as

$$\bar{h} \leq \frac{2\epsilon(1-2\nu)}{\beta \gamma_1}, \qquad \text{(A.8)}$$

which is feasible when $\nu < \frac{1}{2}$. Then, it follows from (A.3) that ν must satisfy

$$\epsilon + \frac{5}{3} n \bar{h} \;=\; \epsilon + \frac{\frac{10}{3} n \epsilon (1-2\nu)}{\beta \gamma_1} \leq \frac{\nu}{\beta \gamma_2} \Longrightarrow \nu \geq \frac{\epsilon(\frac{10}{3} n \gamma_2 + \beta \gamma_1 \gamma_2)}{\gamma_1 + \frac{20}{3} n \epsilon \gamma_2},$$

which is consistent with the condition $\nu < \frac{1}{2}$ for a sufficiently small ϵ. If $\bar{h}$, ϵ, and ν are selected such that (A.3), (A.8), (A.9) are satisfied, then

$$||x_1 - x^*|| \leq \epsilon \Longrightarrow x_1 \in \mathcal{N}(x^*, \epsilon)$$

and (A.4) and (A.5) holds for H_1 as well. Induction on $k+1$ goes similarly, and yields

$$||x_{k+1} - x^*|| \leq c^{k+1} ||x_0 - x^*|| + \bar{h}\delta \sum_{n=0}^{n=k} c^n. \qquad \text{(A.9)}$$

where $c := \frac{\nu}{1-\nu}$ and $\delta := \frac{\beta \gamma_1}{2(1-\nu)}$. Because $\nu < \frac{1}{2} \Longrightarrow c < 1$, the sum in (A.9) converges to $\sum_{n=0}^{n=\infty} c^n = \frac{1}{1-c}$ and $\lim_{k \to \infty} ||x_k - x^*|| = \mathcal{O}(\bar{h})$. □

APPENDIX B
NORMS OF THE MATRICES IN (5.53)-(5.55)

We recall that Q_α in (5.27) and R in (5.45) is,

$$Q_\alpha = \Delta(m_\alpha) \text{ and } R = \Delta(r). \tag{B.1}$$

Noting from (5.31) that $(n-1)\nu = \frac{n-\sqrt{n}}{n} < 1$, we obtain $||\Delta(n)||_\infty = 2 - 2\frac{n-\sqrt{n}}{n(n-1)}$, which reveals that

$$\sqrt{2} \leq ||\Delta(n)||_\infty \leq 2, \ n = 2, 3, \cdots . \tag{B.2}$$

• $||\mathbf{CR\Sigma}||_\infty = ||\mathbf{RM_a^{-1}\Sigma}||_\infty$: We note from (2.1), (5.25) and (5.40) that, $||M_a^{-1}||_\infty = 1/m$ and $||\Sigma||_\infty = \gamma^E$. Therefore, using (B.1) and (B.2), we conclude that

$$||RM_a^{-1}\Sigma||_\infty \leq ||R||_\infty ||M_a^{-1}||_\infty |\Sigma||_\infty \leq \frac{2\gamma^E}{m}. \tag{B.3}$$

$$\tag{B.4}$$

• $||\mathbf{A}||_\infty = ||\mathbf{QD^I}||_\infty$: Since Q and D^I are block diagonal matrices, so is QD^I; thus we establish its norm using the diagonal blocks $Q_\alpha D_\alpha^I$. We note that j^{th} row of $Q_\alpha D_\alpha^I$ is obtained by multiplying each row of D by the entries in the j^{th} row of Q_α and adding them. Without loss of generality, we assume that the node with the smallest number of links $c_\alpha^I := \min_i\{c_{\alpha i}^I\}$ corresponds to the first row of D_α^I, it is the positive end in all of its links, and its links constitute the first c_α^I columns of D_α^I. Then, the first row of $Q_\alpha D_\alpha^I$ is

$$\begin{aligned} 1^{st} \text{ row of } Q_\alpha D_\alpha^I = \quad & (-1 + (m_\alpha - 1)\nu) \times \ 1^{st} \text{ row of } D_\alpha^I \\ + \quad & (1-\nu) \times \ 2^{nd} \text{ row of } D_\alpha^I \\ + \quad & \nu \times \ 3^{rd} \text{ row of } D_\alpha^I \\ \vdots & \\ + \quad & \nu \times \ m_\alpha^{th} \text{ row of } D_\alpha^I. \end{aligned} \tag{B.5}$$

Since the first row of D^I_α has the smallest number of internal links c^I_α, other rows of D^I_α have at least c^I_α nonzero (1 or -1) terms. Then we obtain the first row of $Q_\alpha D^I_\alpha$ as

$$1^{st} \text{ row of } Q_\alpha D^I_\alpha = [-2+m_\alpha\nu, \underbrace{-1+m_\alpha\nu,\ -1+m_\alpha\nu, ...}_{c^I_\alpha - 1 \ terms}, \underbrace{...,1-\nu+\nu,\ 0,\ -1+\nu-\nu,...,-1+\nu-\nu,\ 1-\nu+\nu,\ 0,...}_{\geq c^I_\alpha \ nonzero \ terms (1 \ or -1)}]$$

Noting that $m_\alpha\nu < 1$ from (5.31) and $(B.1)$, we obtain the norm of the 1^{st} row of $Q_\alpha D^I_\alpha$ as

$$\begin{aligned} |1^{st} \text{ row of } Q_\alpha D^I_\alpha|_\infty &= |-2+m_\alpha\nu| + \underbrace{|-1+m_\alpha\nu| + |-1+m_\alpha\nu| + ...}_{c^I_\alpha - 1 \ terms} \\ &\quad \underbrace{+|1| + |-1| + |-1| + |1| + ...}_{\geq c^I_\alpha \ terms} \\ &\geq c^I_\alpha(2-m_\alpha\nu) \geq c^I(2-m_\alpha\nu) > c^I, \end{aligned}$$

which proves that the absolute sum of the entries in the first row of $Q_\alpha D^I_\alpha$ is greater than c^I, and consequently,

$$||QD||_\infty > c^I. \tag{B.6}$$

• $||\mathbf{B}||_\infty = ||\mathbf{QD^E}||_\infty$: We note from (2.1) and (5.39) that $||D^E||_\infty = c^E$, and using (B.2), obtain the upper bound on $||QD^E||_\infty$ as

$$||QD^E||_\infty \leq ||Q||_\infty ||D^E||_\infty \leq 2c^E. \tag{B.7}$$